Beyond Prostate Adenocarcinoma: Expanding the Differential Diagnosis in Prostate Pathologic Conditions[1]

Yi Li, MD
John Mongan, MD, PhD
Spencer C. Behr, MD
Seema Sud, MBBS
Fergus V. Coakley, MD
Jeffry Simko, MD, PhD
Antonio C. Westphalen, MD, PhD

Abbreviations: ADC = apparent diffusion coefficient, BPH = benign prostatic hyperplasia, H-E = hematoxylin-eosin, PSA = prostate-specific antigen, STUMP = stromal neoplasm of uncertain malignant potential

RadioGraphics 2016; 36:1055–1075

Published online 10.1148/rg.2016150226

Content Codes: GU MR OI

[1]From the Department of Radiology and Biomedical Imaging (Y.L., J.M., S.C.B., A.C.W.) and Department of Pathology (J.S.), University of California, San Francisco, 505 Parnassus Ave, M-391, San Francisco, CA 94143-0628; Department of Radiology, Sir Ganga Ram Hospital, New Delhi, India (S.S.); and Department of Diagnostic Radiology, Oregon Health and Science University, Portland, Ore (F.V.C.). Presented as an education exhibit at the 2014 RSNA Annual Meeting. Received July 20, 2015; revision requested November 3; revision received December 6; accepted January 15, 2016. For this journal-based SA-CME activity, the authors J.M., S.C.B., J.S., and A.C.W. have provided disclosures (see end of article); all other authors, the editor, and the reviewers have disclosed no relevant relationships. **Address correspondence to** A.C.W. (e-mail: *Antonio.westphalen@ucsf.edu*).

SA-CME LEARNING OBJECTIVES

After completing this journal-based SA-CME activity, participants will be able to:

- Identify prostate lesions that do not have the typical appearance of adenocarcinoma, which require further workup for an alternate cause.
- Describe the appearances of several prostate pathologic conditions with distinctive imaging features, such as cystadenoma, mucinous adenocarcinoma, sarcoma, and abscess.
- Identify infectious, inflammatory, or congenital lesions that do not require a workup for malignancy.

See www.rsna.org/education/search/RG.

Recent advances in magnetic resonance (MR) imaging of the prostate gland have dramatically improved the ability to detect and stage adenocarcinoma of the prostate, one of the most frequently diagnosed cancers in men and one of the most frequently diagnosed pathologic conditions of the prostate gland. A wide variety of nonadenocarcinoma diseases can also be seen with MR imaging, ranging from benign to malignant diseases, as well as infectious and inflammatory manifestations. Many of these diseases have distinctive imaging features that allow differentiation from prostate acinar adenocarcinoma. Early recognition of these entities produces a more accurate differential diagnosis and may enable more expeditious clinical workup. Benign neoplasms of the prostate include plexiform neurofibroma and cystadenoma, both of which demonstrate distinctive imaging features. Stromal neoplasms of uncertain malignant potential are rare tumors of uncertain malignant potential that are often difficult to distinguish at imaging from more-malignant prostate sarcomas. Other malignant neoplasms of the prostate include urothelial carcinoma, primary prostatic carcinoid, carcinosarcoma, endometrioid or ductal adenocarcinoma, and mucinous adenocarcinoma. Prostatic infections can lead to abscesses of pyogenic, tuberculous, or fungal origins. Finally, miscellaneous idiopathic disorders of the prostate include amyloidosis, exophytic benign prostatic hyperplasia, and various congenital cysts. Considerable overlap can exist in the clinical history and imaging findings associated with these prostate pathologic conditions, and biopsy is often required for ultimate confirmation of the diagnosis. However, many diagnoses, including cystadenoma, mucinous adenocarcinoma, sarcoma, and abscesses, have distinct imaging features, which can enable the informed radiologist to identify the diagnosis and recommend appropriate clinical workup and management.

Introduction

Recent advances in magnetic resonance (MR) imaging of the prostate gland have dramatically improved the ability to detect and stage prostate adenocarcinoma, one of the most frequently diagnosed cancers in men and the most frequently diagnosed pathologic condition of the prostate gland (1). However, men who are suspected of having prostate cancer may have diseases other than adenocarcinoma, many of which can be identified at prostate MR imaging. As prostate MR imaging becomes integral to the workup and staging of prostate cancer, the ability of radiologists to recognize the full spectrum of prostate pathologic conditions beyond adenocarcinoma is increasingly important.

Nonadenocarcinoma disease of the prostate ranges from benign to malignant disease and includes nonneoplastic infectious and

TEACHING POINTS

- In the setting of cancer, these neurovascular bundles provide a route for extraprostatic spread of malignancy.
- Most sarcomas appear as well-circumscribed masses that are homogeneously hypointense on T1-weighted MR images and heterogeneous on T2-weighted MR images and enhance avidly after contrast material administration. Because of their rapid growth, sarcomas usually contain areas of central necrosis, which may help to distinguish more-aggressive sarcomas from more-benign variants of STUMP.
- Paragangliomas can be distinguished from adenocarcinoma on the basis of their T2 signal intensity, because adenocarcinoma is T2 hypointense. Scintigraphy with iobenguane I 123 (*m*-iodobenzylguanidine) can also be used, which demonstrates localized uptake in the prostate, which is caused by the presence of neuroendocrine receptors.
- Unlike typical adenocarcinoma, mucinous tumors typically appear both T1 and T2 hyperintense because of the proteinaceous fluid content of mucinous adenocarcinomas, but the appearance may vary, depending on the amount of mucin. The T2-hyperintense tumor may be difficult to recognize within the T2-hyperintense background of the peripheral zone. In addition, unlike adenocarcinoma, mucinous adenocarcinoma does not demonstrate abnormalities at diffusion-weighted MR imaging and MR spectroscopic imaging.
- Metastatic involvement of the prostate gland by primary carcinomas of other organs is exceptionally rare and, when found, often arises in the context of direct extension of tumors in adjacent organs or disseminated disease involving multiple organs. Bladder urothelial carcinoma is the most common cancer to involve the prostate because of its proximity to the prostate gland. Colorectal cancer is next most frequent but is much less common.

inflammatory processes. Accurate diagnosis of these entities may prevent further unnecessary invasive procedures, influence subsequent testing, and help determine the final pathologic diagnosis. Ultimately, a more precise differential diagnosis that is based on imaging findings leads to more accurate and expeditious clinical management.

The purpose of this article is to describe the MR imaging appearance of less-common prostate diseases and how to differentiate these diseases from adenocarcinoma. First, the anatomic structure of the prostate gland and its morphologic and functional assessment with MR imaging are described, along with the MR imaging appearances of nonadenocarcinoma disease. A variety of prostatic neoplasms are covered, followed by several benign disorders, including various infections.

Prostate Anatomy

Anatomically, from centrally to peripherally, the prostate is divided into four distinct zones: *(a)* the transition zone surrounding the prostatic urethra, which, in a population of young men, contains approximately 5% glandular tissue; *(b)* the central zone, which contains 20% glandular tissue; *(c)* the outer peripheral zone, which contains 70%–80% glandular tissue; and *(d)* the anterior fibromuscular stroma, which contains no glandular tissue (2). Prostate adenocarcinoma most commonly arises in the peripheral zone.

The neurovascular bundles are located posterolateral to the prostate bilaterally and penetrate into the prostate at the apex and base. These bundles consist of cavernous nerves responsible for erectile function, arterial branches of the inferior vesicle artery, and veins. In the setting of cancer, these neurovascular bundles provide a route for extraprostatic spread of malignancy.

Morphologic and Functional MR Imaging Assessment of the Prostate

The current standard for imaging men who are suspected of having prostate cancer is multiparametric MR imaging, which includes T1-weighted MR imaging, high-resolution T2-weighted MR imaging, diffusion-weighted MR imaging, dynamic contrast material–enhanced MR imaging, and, in some institutions, MR spectroscopic imaging.

T1-weighted pulse sequences are primarily used to detect postbiopsy hemorrhage, to assess for invasion of surrounding periprostatic fat, or to serve as the baseline for contrast-enhanced images. Most lesions are isointense to the normal prostatic tissue on T1-weighted MR images.

On T2-weighted MR images, the normal peripheral zone appears hyperintense, and the transition zone is typically heterogeneous secondary to benign prostatic hyperplasia (BPH). Most diseases, including adenocarcinomas, predominantly demonstrate low T2 signal intensity.

Although diffusion-weighted MR imaging is considered one of the main sequences for assessment of adenocarcinomas of the prostate, other processes can also be identified and characterized on the basis of their diffusion characteristics. Tumor typically demonstrates restricted diffusion secondary to high cellularity. Restricted diffusion, however, is not specific for tumor and may also be seen with other processes, such as an abscess or stromal BPH (3,4).

Dynamic contrast-enhanced MR imaging is performed on the basis of the theory that adenocarcinomas manifest with marked angiogenesis and permeative vessels and, therefore, demonstrate a high rate of extracellular contrast material diffusion, which leads to early hyperenhancement and rapid washout of contrast material. The findings from recent research have demonstrated that this pattern, however, is not unique to adenocarcinoma and may also be seen with benign peripheral zone tissue (5).

World Health Organization Histologic Classification of Tumors of the Prostate

Epithelial tumors
Glandular neoplasms
Adenocarcinoma (acinar)
Carcinoma with spindle cell differentiation (carcinosarcoma, sarcomatoid carcinoma)
Prostatic intraepithelial neoplasia (PIN)
PIN, grade III (PIN III)
Ductal adenocarcinoma
Urothelial tumors
Urothelial carcinoma
Squamous tumors
Adenosquamous carcinoma
Squamous cell carcinoma
Basal cell tumors
Basal cell adenoma
Basal cell carcinoma
Neuroendocrine tumors
Endocrine differentiation within adenocarcinoma
Carcinoid tumor
Small cell carcinoma
Paraganglioma
Neuroblastoma
Prostatic stromal tumors
Stromal tumor of uncertain malignant potential (STUMP)
Stromal sarcoma
Mesenchymal tumors
Leiomyosarcoma
Rhabdomyosarcoma
Chondrosarcoma
Angiosarcoma
Malignant fibrous histiocytoma
Malignant peripheral nerve sheath tumor
Hemangioma
Chondroma
Leiomyoma
Granular cell tumor
Hemangiopericytoma
Solitary fibrous tumor
Miscellaneous tumors
Cystadenoma
Nephroblastoma
Rhabdoid tumor
Germ cell tumor
Choriocarcinoma
Clear cell adenocarcinoma
Melanoma
Hematolymphoid tumors
Lymphoma
Leukemia

Source.—Reference 6.

MR spectroscopic imaging uses the characteristic chemical shift of biochemical compounds to measure their relative concentrations. In many prostate pathologic conditions and, in particular, cancers, the citrate peak at 2.6 ppm will be decreased, and the choline peak at 3.2 ppm will be elevated.

MR Imaging Appearance of Nonadenocarcinoma Disease

Nonadenocarcinoma disease of the prostate can be broadly categorized into neoplasms (covering a spectrum from benign to malignant), infectious diseases, and other disorders, which include amyloidosis, congenital anomalies, and BPH.

Prostatic Neoplasms

A wide variety of neoplasms occur in the prostate, both benign and malignant. The World Health Organization's histologic classification of tumors (Table) (6) categorizes them by cellular origin: epithelial, neuroendocrine, prostatic stromal, mesenchymal, miscellaneous, and hematolymphoid. In the following paragraphs, we will look at some of the most common and distinctive prostatic neoplasms, with an emphasis on how their imaging appearances differ from that of usual acinar adenocarcinoma.

Cystadenoma

Prostatic cystadenoma is a rare benign tumor characterized histologically by cysts and glands lined by cuboidal epithelium, all within a fibrous stroma (7). Most patients initially present with urinary obstruction or a palpable abdominal mass, although some patients are asymptomatic in the early stages and are seen after screening discloses an increased level of prostate-specific antigen (PSA). The diagnosis is usually established after excisional biopsy, and the prostatic origin of the lesion can be confirmed by positive staining of the epithelial cells for PSA (8). Aspiration of these cysts usually yields hemorrhagic fluid and histiocytes but no malignant cells (9).

At MR imaging, cystadenomas appear as multilocular T2-hyperintense cystic lesions with surrounding isointense soft tissue. Variations in T2 signal intensity and the presence of fluid-fluid levels are suggestive of secondary hemorrhage (Fig 1). These lesions can grow to large proportions, often occupying the entire pelvis at the level of the bladder. The tumor causes appreciable mass effect but does not invade adjacent structures. Local invasion of surrounding structures should be suggestive of alternate malignant causes. Prostatic cystadenomas can be distinguished from adenocarcinoma on the basis of their large size and the presence of multilocular

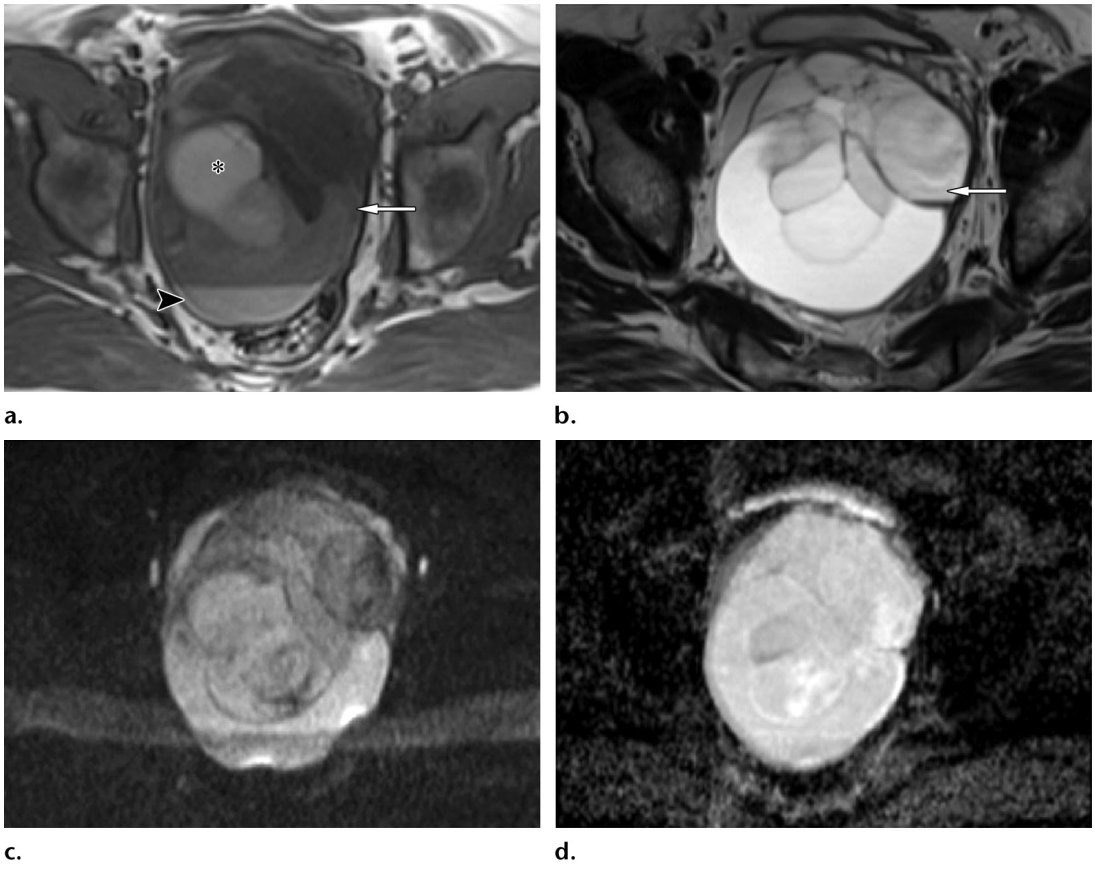

Figure 1. Giant cystadenoma of the prostate in a 36-year-old man. **(a, b)** Axial T1-weighted **(a)** and T2-weighted **(b)** MR images show a large multilocular cystic mass (arrow) with heterogeneous signal intensity. The high signal intensity on **a** reflects the presence of mucin (∗ on **a**) and layering blood (arrowhead on **a**). **(c, d)** Axial diffusion-weighted MR image **(c)** and the apparent diffusion coefficient (ADC) map **(d)** show no restricted diffusion. The patient underwent fine-needle aspiration biopsy and then surgery, and the histopathologic findings helped confirm the diagnosis.

cysts. Differential considerations include hydatid parasitic infection or a cystic carcinoma.

Despite the benign nature of cystadenoma, resection is often performed for symptomatic relief and confirmation of diagnosis. However, lesions tend to recur if resection is incomplete.

Stromal Tumor of Uncertain Malignant Potential

STUMPs are rare proliferative lesions of the prostatic stroma that have specific histologic and immunohistologic features that distinguish them from prostate sarcoma. Several subtypes of STUMPs exist; these display a wide range of biologic behaviors and have an unpredictable clinical course (10,11). Some lesions cause only local mass effect and adherence (primarily to the rectum), and others are associated with aggressive local invasion and metastases and have a high rate of recurrence after resection. Diagnosis is made with the findings from biopsy and histopathologic examination (Fig 2e).

At T1- and T2-weighted MR imaging, STUMP appears as a large well-circumscribed heterogeneous lesion with predominantly low signal intensity, which may arise from any prostatic zone (Fig 2a–2d). STUMP is distinguishable from adenocarcinoma on the basis of its size and heterogeneity. It is difficult to differentiate a STUMP from a prostate sarcoma, and less-aggressive forms of STUMP may even mimic BPH nodules. Thus, in patients who appear to have a particularly large or aggressive form of BPH nodule, biopsy is warranted to exclude STUMP. Although the natural history and prognosis of STUMP are still unclear, most patients undergo surgical resection because of the potential for aggressive disease.

Sarcoma

Prostate sarcomas are rare tumors, accounting for approximately 0.1%–0.2% of all primary prostatic neoplasms (6). Sarcomas are primarily of mesenchymal origin but, rarely, can arise from the prostatic stroma. Patients often present with rapid onset of urinary obstruction or a palpable mass.

Most sarcomas appear as well-circumscribed masses that are homogeneously hypointense on T1-weighted MR images and heterogeneous on T2-weighted MR images and enhance avidly after

Figure 2. STUMP in a 40-year-old man who presented with gross hematuria. The patient underwent digital rectal examination and a computed tomographic (CT) examination, which disclosed a large nodule on the left side of his prostate. At transrectal ultrasonography (US)–guided biopsy, a STUMP was diagnosed. MR imaging was performed for treatment planning. **(a)** Axial T2-weighted MR image shows a large lesion (arrow) that is centered in the left anterior midportion of the gland. The lesion is circumscribed and heterogeneous, with predominantly low signal intensity. **(b, c)** Axial diffusion-weighted MR image **(b)** and ADC map **(c)** show moderately restricted diffusion (arrow) within the lesion. **(d)** Axial contrast-enhanced MR image shows that the lesion enhances homogeneously (arrow) after administration of gadolinium-based contrast material. **(e)** Photomicrograph shows a proliferation of bland spindle cells between dense bands of collagen (arrow), with no increased mitotic activity or branching vascularity. (Hematoxylin-eosin [H-E] stain; original magnification, ×200.)

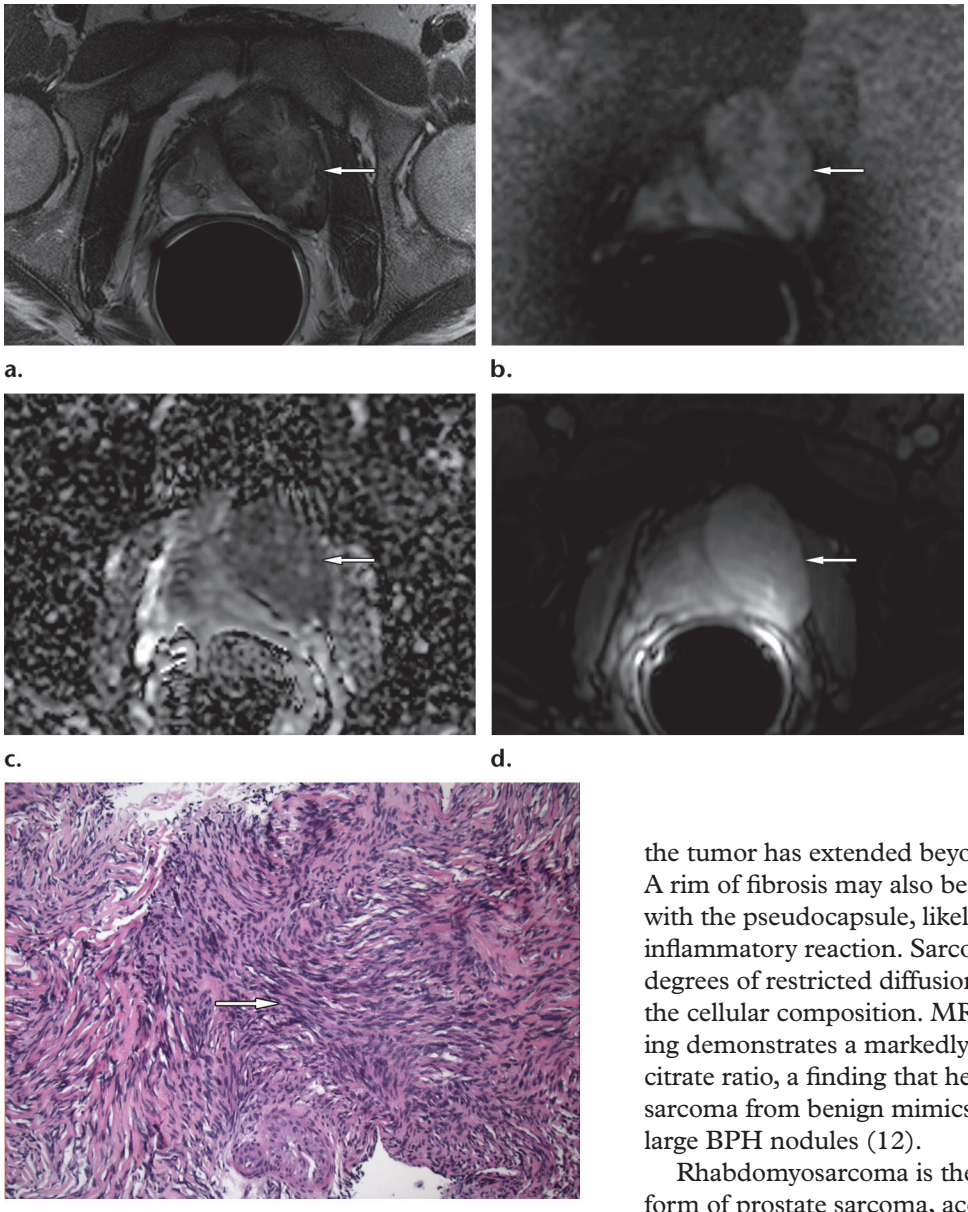

contrast material administration. Because of their rapid growth, sarcomas usually contain areas of central necrosis, which may help to distinguish more-aggressive sarcomas from more-benign variants of STUMP. Many sarcomas demonstrate a partial or complete T2-hypointense pseudocapsule that represents the interface between the tumor and adjacent compressed periprostatic fat, where the tumor has extended beyond the prostate (12). A rim of fibrosis may also be seen in association with the pseudocapsule, likely the result of an inflammatory reaction. Sarcomas have varying degrees of restricted diffusion that are based on the cellular composition. MR spectroscopic imaging demonstrates a markedly elevated choline-to-citrate ratio, a finding that helps to differentiate sarcoma from benign mimics, such as unusually large BPH nodules (12).

Rhabdomyosarcoma is the most common form of prostate sarcoma, accounting for 42% of all cases, and primarily occurs in children and adolescents. Leiomyosarcoma is the second most prevalent form, accounting for 25% of sarcomas, and is the most common form of prostate sarcoma in adults. Although most prostate sarcomas are similar in appearance and although the final distinction of subtype is ultimately based on histologic findings, several imaging features may help to distinguish the various sarcomas. Embryonal rhabdomyosarcomas typically manifest as large lobulated masses, often protruding into the bladder

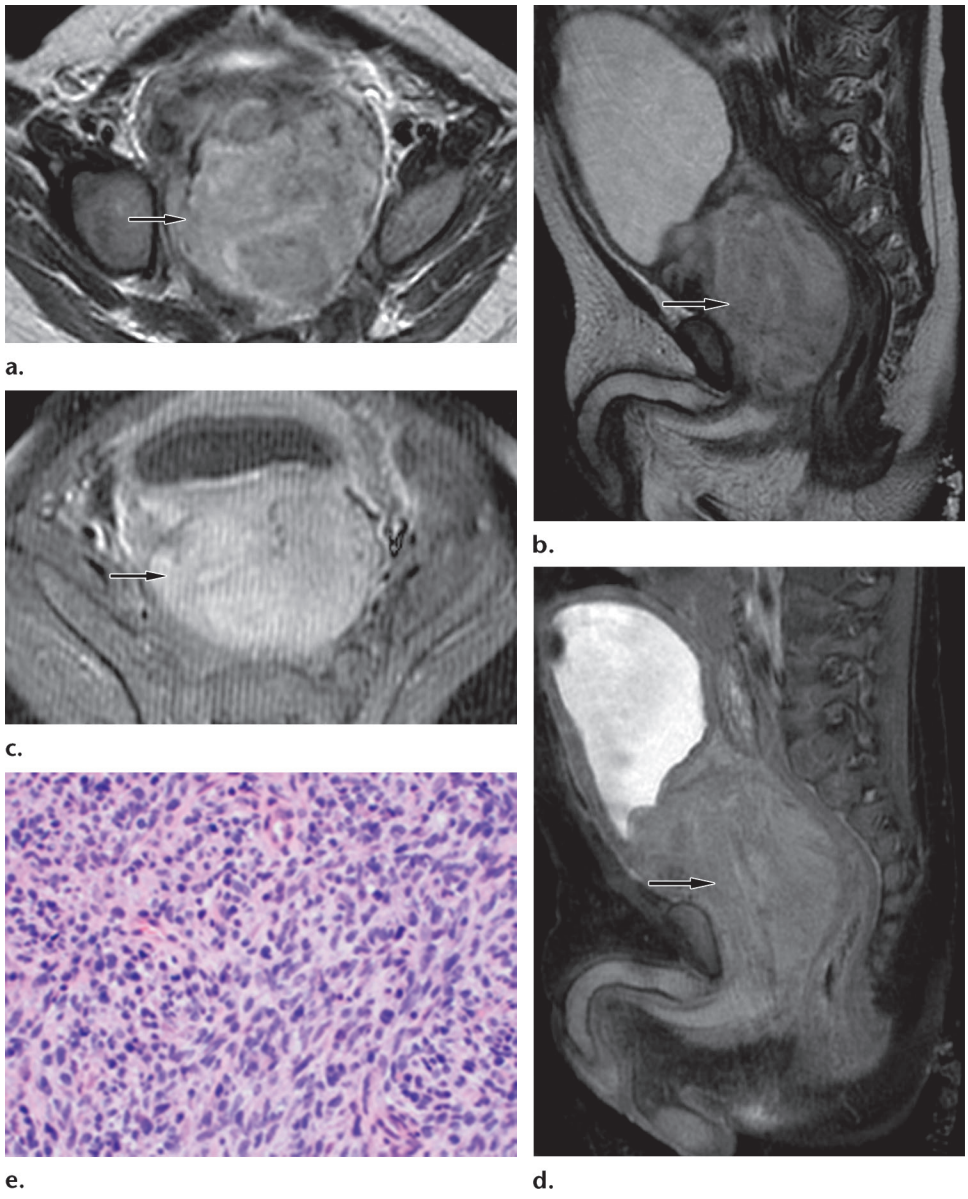

Figure 3. Embryonal rhabdomyosarcoma in a 4-month-old boy who presented with a palpable pelvic mass. The patient underwent imaging evaluation, including MR imaging. **(a, b)** Axial **(a)** and sagittal **(b)** T2-weighted MR images show a large mildly hyperintense heterogeneous mass (arrow) replacing the entire gland. **(c, d)** Axial **(c)** and sagittal **(d)** contrast-enhanced fat-saturated T1-weighted MR images show mostly homogeneous enhancement of the tumor (arrow). At transrectal US–guided biopsy, rhabdomyosarcoma was diagnosed. **(e)** Photomicrograph shows a small round blue cell tumor with ample eosinophilic cytoplasm and variably round to spindle cells. (H-E stain; original magnification, ×400.) The patient underwent radical prostatectomy and chemotherapy.

lumen (Fig 3). Alveolar rhabdomyosarcomas, a more-aggressive subtype, usually appear more infiltrative and less well defined. Leiomyosarcomas often manifest with early pulmonary and hepatic metastases (Fig 4). Prostate sarcomas are rarely confused with adenocarcinoma, given their large size and heterogeneous appearance and, in the case of rhabdomyosarcoma, their manifestation in a different age group. Regardless of subtype, the prognosis is often poor because of early metastasis (13).

Urothelial Carcinoma

Urothelial carcinoma, or transitional cell carcinoma, can occur as a primary cancer of the prostate gland, arising from the prostatic ducts or acini, and urothelial carcinoma accounts for 2%–4% of all prostate cancers. More commonly, it is seen as a synchronous or metachronous tumor associated with urothelial carcinoma of the bladder or urethra (9). Pathologically, many cases demonstrate elements of both prostatic urothelial carcinoma and adenocarcinoma.

At our institution, a patient who had prostatic urothelial carcinoma diagnosed from the findings at histopathologic examination initially presented with a mildly T2-hyperintense infiltrative tumor, with avid enhancement after contrast material administration (Fig 5). T2 hyperintensity allows differentiation from acinar adenocarcinoma, which is typically T2 hypointense. The presence of synchronous tumors elsewhere in the genitourinary system also makes urothelial carcinoma more likely. These tumors carry a poor prognosis, with a mean survival of 17–23 months and a 5-year survival rate of approximately 37%, depending on the stage of disease at diagnosis (14).

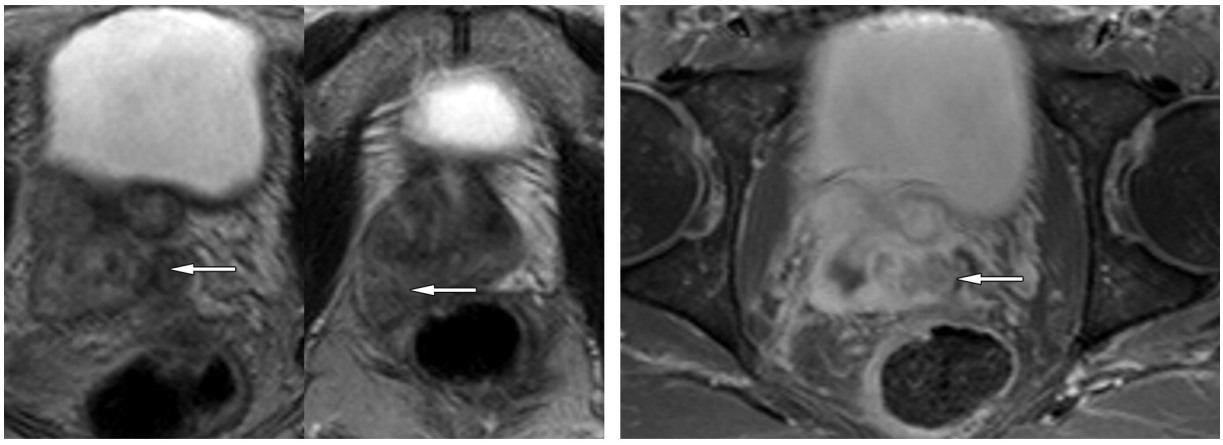

a. b.

Figure 4. Leiomyosarcoma of the prostate in a 45-year-old man. **(a)** Two axial sequential T2-weighted MR images (image at left obtained more cephalad than image at right) show a large lobulated heterogeneous mass (arrows) arising from the right midportion of the gland and extending to the base. **(b)** Axial contrast-enhanced MR image of the tumor shows avid and heterogeneous enhancement with areas of central necrosis (arrow). The patient underwent radical prostatectomy and partial cystectomy, as well as radiation therapy.

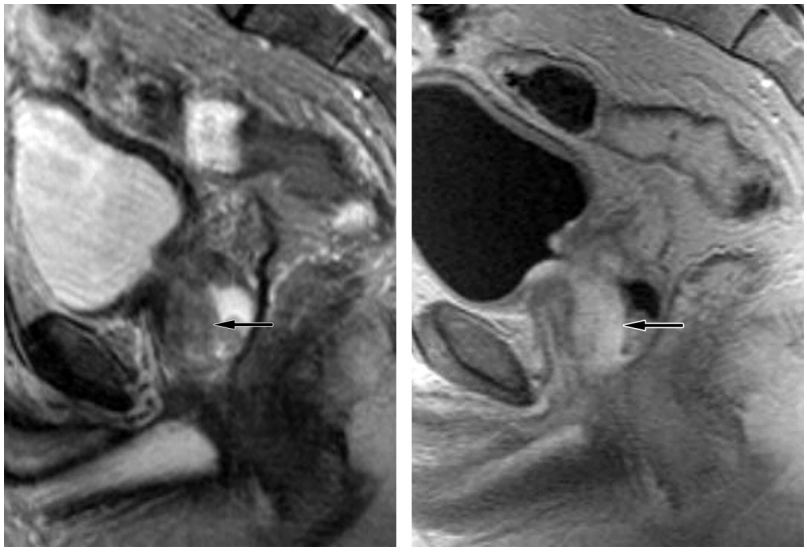

a. b.

Figure 5. Urothelial carcinoma, or transitional cell carcinoma, of the prostatic urethra diagnosed at transurethral resection of the prostate in a 55-year-old man. MR imaging of the pelvis was ordered to evaluate for metastatic disease after BCG infusion therapy. Sagittal T2-weighted **(a)** and contrast-enhanced T1-weighted **(b)** MR images show an infiltrative tumor located predominantly in the anterior aspect of the gland. The tumor has a higher T2 signal intensity (arrow on **a**) than that of muscle and enhances avidly (arrow on **b**) after administration of gadolinium-based contrast material.

Prostatic Carcinoid

Primary prostatic carcinoid is extremely rare and is thought to represent one of four major manifestations of neuroendocrine malignancy in the prostate gland (prostatic carcinoid, small cell carcinoma, large cell neuroendocrine carcinoma, and focal neuroendocrine differentiation in prostate adenocarcinoma) (15). Neuroendocrine cells are scattered in all anatomic zones of the prostate but typically represent less than 1% of the prostatic glandular epithelium (16). Primary prostatic carcinoid tumors show true neuroendocrine differentiation and classic histologic features of carcinoid tumors, with chromogranin A and synaptophysin immunoreactivity (9).

Unlike patients with typical acinar adenocarcinoma, patients with prostatic carcinoid do not present with an elevated PSA level. Some tumors, historically called "carcinoid-like tumors," demonstrate histologic features of acinar adenocarcinoma as well as focal neuroendocrine immunoreactivity, and these tumors express neuroendocrine markers and demonstrate elevation of the PSA level (15). Clinically, these carcinoid-like tumors behave similarly to adenocarcinoma. In contrast, prostatic carcinoid tumors have been described as fairly indolent lesions, although characterization of their natural history has been limited by their rarity (15,17).

At our institution, a patient with known carcinoid tumor that had been diagnosed from the findings at histopathologic examination subsequently had a large heterogeneous mass with mild T2 hyperintensity identified at a restaging CT examination (Fig 6). In other case reports in the literature, investigators have described

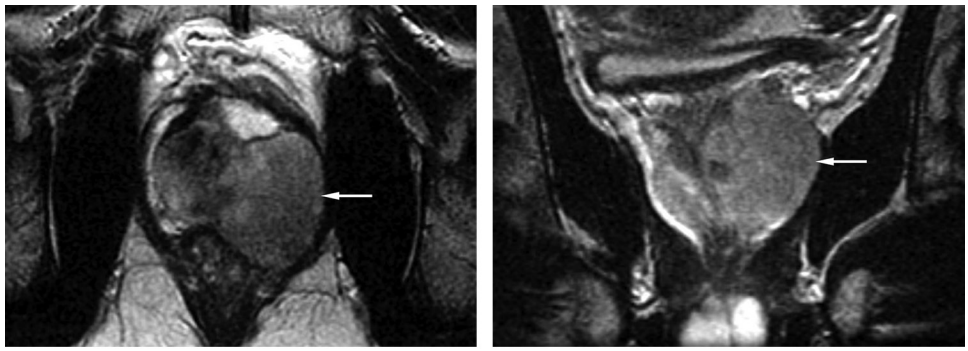

a. b.

Figure 6. Prostatic carcinoid in a 38-year-old man with known carcinoid. A prostatic mass was identified at a posttreatment CT examination performed for restaging, and an MR imaging examination was ordered for further evaluation. Axial **(a)** and coronal **(b)** T2-weighted MR images show a large slightly heterogeneous hyperintense mass (arrow) involving the left side of the prostate from the apex to the base.

similar findings (17,18). Prostatic carcinoid may be distinguished from typical acinar adenocarcinoma on the basis of its size and mild T2 hyperintensity. Distinguishing carcinoid from other rare tumors such as STUMP or sarcoma is more difficult, and the final diagnosis is made at histopathologic examination.

Paraganglioma

Paragangliomas are extra-adrenal pheochromocytomas and develop from extra-adrenal chromaffin cells. Prostatic paragangliomas are exceedingly rare, with less than a dozen cases reported to date (19). Prostatic paraganglioma arises from the parasympathetic tissue adjacent to and behind the prostate gland and is associated with several familial syndromes, including multiple endocrine neoplasia IIA and IIB, neurofibromatosis 1, von Hippel-Lindau syndrome, Carney complex (Carney triad), and familial paraganglioma (20).

Patients with functional tumors often present differently from patients with other prostatic neoplasms. Many patients with paragangliomas present with the classic triad of symptoms associated with catecholamine production: headache, tachycardia, and sweating. These symptoms may be exacerbated or instigated by micturition or the digital rectal examination. In contrast, patients with nonfunctional tumors generally present with symptoms that mirror those of other prostate pathologic conditions, including hematuria and obstructive uropathy.

At prostate MR imaging, paragangliomas often appear as mildly T2-hyperintense lobulated masses, with avid enhancement after contrast material administration. Paragangliomas can be distinguished from adenocarcinoma on the basis of their T2 signal intensity, because adenocarcinoma is T2 hypointense (Fig 7). Scintigraphy with iobenguane I 123 (*m*-iodobenzylguanidine) can also be used, which demonstrates localized uptake in the prostate, which is caused by the presence of neuroendocrine receptors (21).

Definitive diagnosis of paraganglioma is made at biopsy, with positive staining for synaptophysin, neurofilament, neuron-specific enolase, and S-100 protein. Tumors will show a negative staining reaction for PSA. In the absence of metastatic disease, it is difficult to determine on the basis of histologic findings whether the paraganglioma is benign or malignant, and definitive management requires radical prostatectomy.

Sarcomatoid Carcinoma and Carcinosarcoma

Sarcomatoid carcinomas are rare biphasic tumors that demonstrate admixtures of high-grade epithelial cancer and sarcomatoid components, and these carcinomas account for less than 0.1% of prostate cancers (22). Only about 100 cases have been reported in the literature (23). These cancers are postulated to represent either a collision of epithelial and mesenchymal elements or a treatment-driven mutation of an underlying adenocarcinoma into a lesion with sarcomatoid features (24). Histologically, the tumors demonstrate an admixture of sarcomatous and carcinomatous elements, with the carcinomatous elements usually manifest in the form of a high-grade adenocarcinoma (Fig 8f, 8g). *Carcinosarcoma* is a term synonymous with the heterologous subtype of sarcomatoid carcinoma, in which the sarcomatous elements exhibit differentiation along the lines of specific mesenchymal cells.

At our institution, a patient with prostate carcinosarcoma diagnosed from the findings at histologic examination had initially presented with a mass that was heterogeneously T2 hyperintense at MR imaging (Fig 8a–8e), with lobulation and areas of central cystic degeneration. Contrast-enhanced images demonstrated early heterogeneous enhancement. In other reports of prostate

Figure 7. Paraganglioma in a 27-year-old man who presented with a history of a 10-kg (22-lb) weight loss during the preceding 4 months, an increased appetite, and the need to eat 4000 calories/day to maintain his weight. A CT examination was ordered, which disclosed a large lobulated prostate. MR imaging was performed for further evaluation. **(a, b)** Axial **(a)** and coronal **(b)** T2-weighted MR images show a lobulated hyperintense mass (arrow) located in the anterior aspect of the prostate. **(c)** Axial contrast-enhanced MR image shows that the mass (arrow) enhances avidly. In view of the clinical presentation and other biochemical markers, the patient was suspected of having a paraganglioma, and scintigraphy with iobenguane I 123 was performed. **(d)** Scintigraphic image obtained with iobenguane I 123 shows marked prostatic uptake (arrow). The patient underwent prostatectomy. **(e)** Photograph of the macroscopic specimen from prostatectomy shows the mass (*). **(f)** Photomicrograph shows positive staining reaction for synaptophysin (arrow). (Synaptophysin stain; original magnification, ×400.) **(g)** Photomicrograph shows positive staining reaction for chromogranin (arrow). (Chromogranin stain; original magnification, ×400.) The findings at histologic evaluation were also positive for neuron-specific enolase (not shown). The results of immunohistochemical analysis were negative for multiple other markers, including pancytokeratin, cytokeratin 903 (CK903), CK7, CK20, epithelial membrane antigen, PSA, prostatic acid phosphatase, HMB45, P504S, and thyroid transcription factor-1. **(h)** Photomicrograph shows tumor cells with moderate amounts of cytoplasm and small nuclei, arranged in compact aggregates (arrow). (H-E stain; original magnification, ×400.)

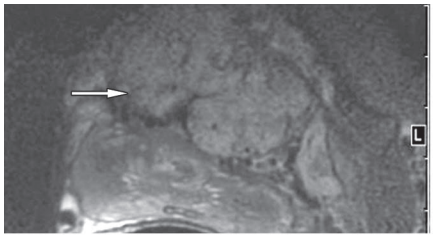

a.

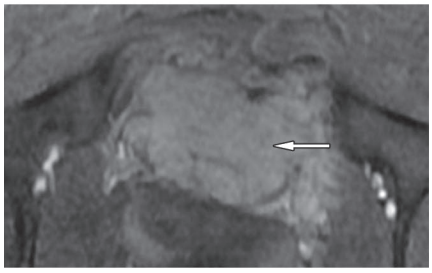

c.

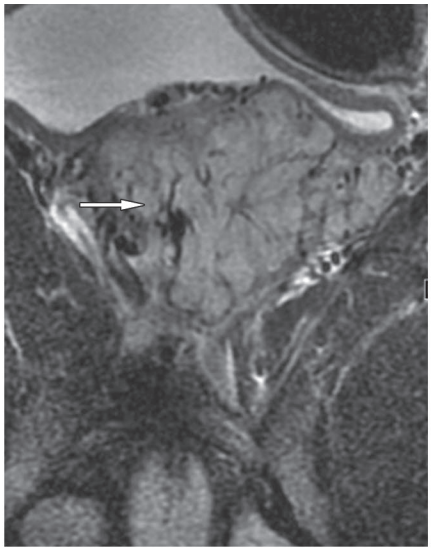

b.

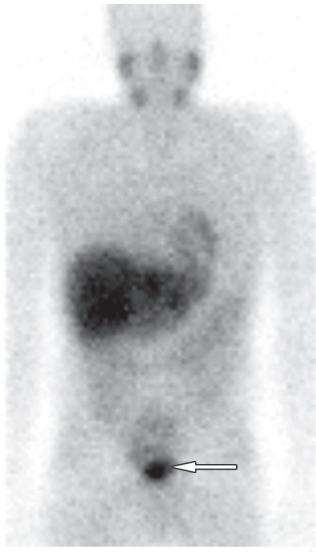

d.

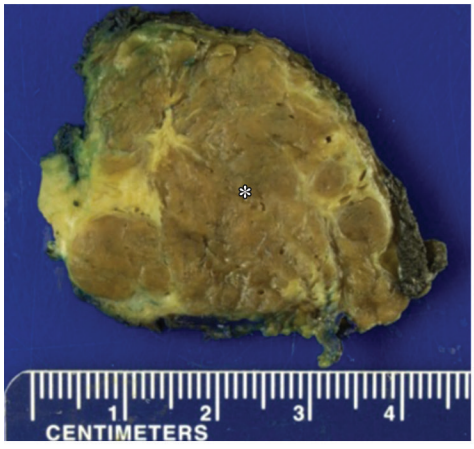

e.

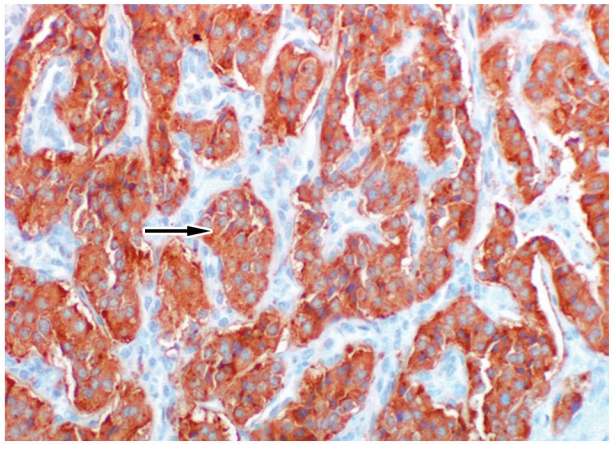

f.

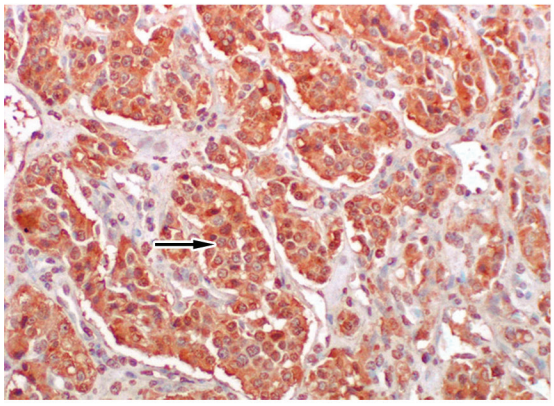

g.

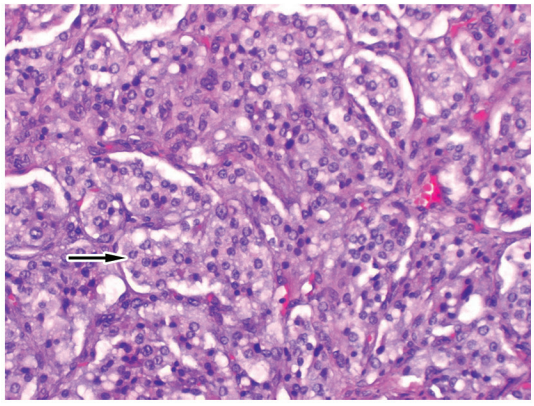

h.

Figure 8. Prostate adenocarcinoma admixed with spindle cell sarcoma (Gleason score, 4 + 4) in a 68-year-old man. The patient presented with progressive difficulty in voiding, which was initially evaluated with cystoscopy and a CT examination. An MR imaging examination was requested for further evaluation. **(a)** Axial T2-weighted MR image shows a large lobulated heterogeneously hyperintense mass (*) with an associated cystic component (arrow) that replaces the normal prostatic tissue. Note the fluid-fluid level related to a small volume of old hemorrhage (arrowhead). **(b, c)** Axial diffusion-weighted MR image **(b)** and ADC map **(c)** of the tumor show mildly restricted diffusion (*). **(d)** Axial dynamic contrast-enhanced MR image shows early and heterogeneous enhancement of the solid component of the mass (*) distant from the cystic area. The cystic component, likely the result of necrosis related to rapid tumor growth outpacing neovascularity, does not demonstrate enhancement (arrow). **(e)** MR spectroscopic image shows malignant metabolism in parts of the mass (within black rectangle); the paired numbers in the boxes (choline-to-creatine ratio on top; ratio of choline plus citrate to creatine on bottom) in the grid at right represent malignant peaks correlating with the areas in the boxes within the black rectangle. The patient underwent open prostatectomy with lymph node dissection and cystectomy with a sigmoid conduit, abdominal perineal resection of the rectum, and intraoperative radiation therapy *(Fig 8 continues)*.

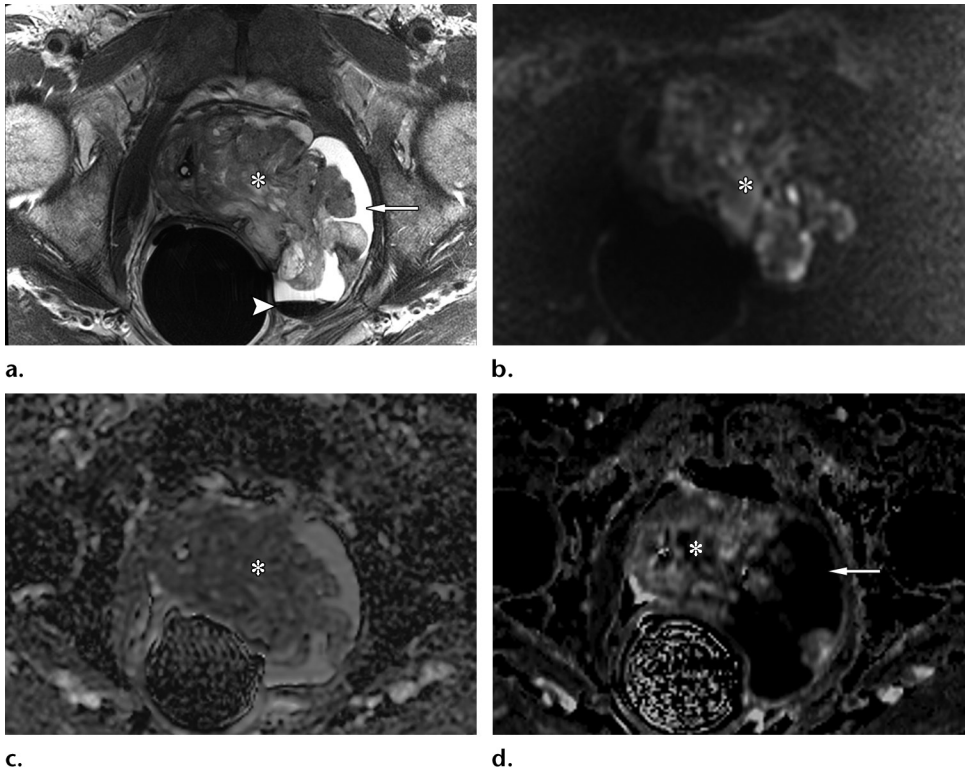

carcinosarcoma in the literature, investigators have described a similar appearance (25,26). Sarcomatoid carcinoma can be distinguished from adenocarcinoma on the basis of its size and heterogeneity. Differentiation from other rare prostate tumors can be challenging on the basis of imaging alone, but sarcomatoid carcinoma may be inferred on the basis of a lobulated tumor with areas of cystic change.

Carcinosarcoma is considered one of the most aggressive prostate malignancies, regardless of the form of therapy (22). The mean survival after diagnosis is 7 months (27).

Ductal or Endometrioid Adenocarcinoma

Ductal adenocarcinoma is a rare subtype of prostate adenocarcinoma initially thought to arise from müllerian structures at the verumontanum and prostatic utricle. Embryologically, the utricle is the only part of the male genitourinary system that originates from the müllerian duct; and histologically, the malignancy appears similar to uterine endometrial adenocarcinoma (28,29). Despite the postulated müllerian origins of the tumor, it has a positive staining

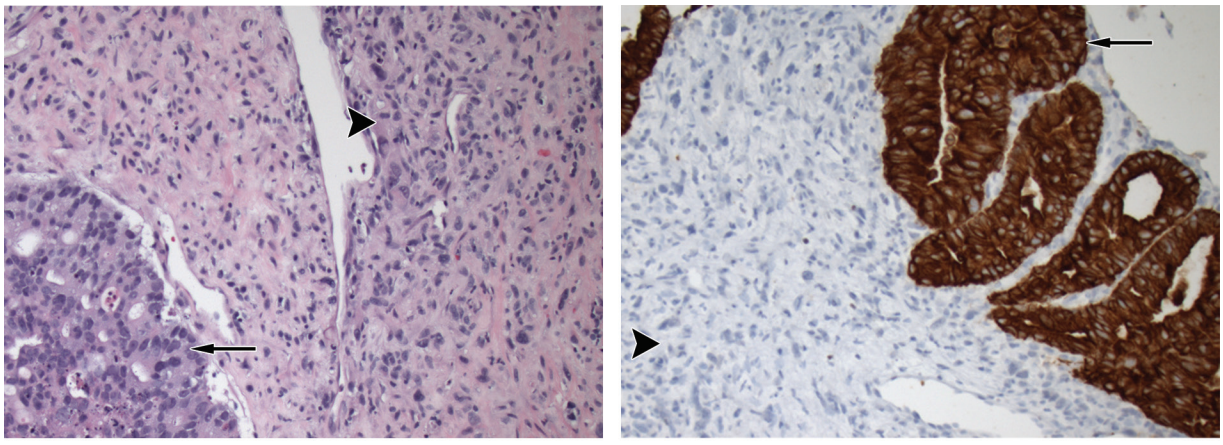

f. g.

Figure 8 *(continued)*. The findings at histologic examination helped confirm the diagnosis of a carcinosarcoma of the prostate. **(f)** Photomicrograph shows areas of glandular tissue, consistent with carcinoma (arrow), and adjacent areas of spindle cells, consistent with sarcoma (arrowhead). (H-E stain; original magnification, ×200.) **(g)** Photomicrograph shows areas of a positive staining reaction for keratin, consistent with carcinoma (arrow). Other areas of a negative staining reaction for keratin, which correspond to areas of spindle cells at H-E staining, represent heterologous sarcoma elements (arrowhead). (Keratin stain; original magnification, ×200.)

reaction for PSA and prostatic acid phosphatase, and patients often present with an elevated PSA level. Ductal carcinoma is the most common histologic variant of prostate carcinoma and is often seen in mixed histologic findings referred to as "ductal-acinar adenocarcinoma." The mixed subtype is more common than pure ductal adenocarcinoma (23).

In many cases in which ductal adenocarcinoma coexists with typical acinar adenocarcinoma, differentiation from acinar adenocarcinoma on the basis of imaging findings may be difficult. Pure ductal adenocarcinoma may manifest as a relatively more distinctive imaging subtype. In one prior report of ductal adenocarcinoma in the literature, investigators described a large heterogeneous mass associated with a multilocular cyst invading the bladder neck (30). In one patient at our institution, whose prostate cancer was diagnosed on the basis of the histopathologic findings at biopsy, MR imaging demonstrated a heterogeneous encapsulated mass with markedly restricted diffusion on the ADC map. No cysts were found in our case (Fig 9).

Specimens of ductal adenocarcinoma from prostatectomies often demonstrate a higher pathologic stage and a higher rate of positive margins and nodal metastases (31). Also, the ductal adenocarcinoma component is usually of high grade (Gleason score, 4). In the results of most studies, the outcomes for patients with ductal adenocarcinoma are worse than those for patients with typical acinar adenocarcinoma, likely secondary to the higher stage and grade of the ductal subtype (23). However, in some reports, investigators have suggested a natural history similar to that of acinar adenocarcinoma. The apparent discrepancy in the reported natural history of this disease may be caused by the inclusion of tumors of mixed histologic findings in some series (32).

Mucinous Adenocarcinoma

Mucinous adenocarcinoma, another rare variant of prostate adenocarcinoma, is seen in approximately 0.4% of prostatic surgical specimens (33). Because a majority of prostate adenocarcinomas contain some mucinous material, the distinction of the mucinous subtype is made when more than 25% of the tumor contains clusters of cells floating in lakes of mucin (Fig 10) (34). The diagnosis is often difficult to make at biopsy because of the paucity of cells that are obtained.

Given the rarity of the diagnosis of mucinous adenocarcinoma and the potential for biopsy sampling error, recognition of this entity at MR imaging plays an important role in its diagnosis. Unlike typical adenocarcinoma, mucinous tumors typically appear both T1 and T2 hyperintense because of the proteinaceous fluid content of mucinous adenocarcinomas, but the appearance may vary, depending on the amount of mucin (Fig 10) (9). The T2-hyperintense tumor may be difficult to recognize within the T2-hyperintense background of the peripheral zone. In addition, unlike adenocarcinoma, mucinous adenocarcinoma does not demonstrate abnormalities at diffusion-weighted MR imaging and MR spectroscopic imaging (35).

Originally thought to be more aggressive than typical acinar adenocarcinoma, mucinous adenocarcinoma is now believed to have a comparable, if not more favorable, prognosis. In the largest

Figure 9. Ductal or endometrioid carcinoma (Gleason score, 4 + 3) in the left apex of the prostate in a 58-year-old man, a finding that was diagnosed at histopathologic examination. An MR imaging examination was ordered for staging and treatment planning. **(a)** Axial T2-weighted MR image shows a heterogeneous encapsulated nodule (arrow) in the peripheral zone of the left apex. **(b)** ADC map shows markedly restricted diffusion (arrow) in the nodule. No abnormalities were seen at MR spectroscopic imaging (not shown). Dynamic contrast-enhanced MR imaging was not performed because of the patient's low glomerular filtration rate. Two months after imaging, the patient underwent prostatectomy. Histopathologic sections showed tumor within the left apex. **(c)** Photomicrograph shows cells with enlarged and hyperchromatic nuclei arranged in a papillary and glandular configuration, lined by variable stratified columnar epithelium (arrow), findings that helped establish the diagnosis of ductal or endometrioid carcinoma. (H-E stain; original magnification, ×200.)

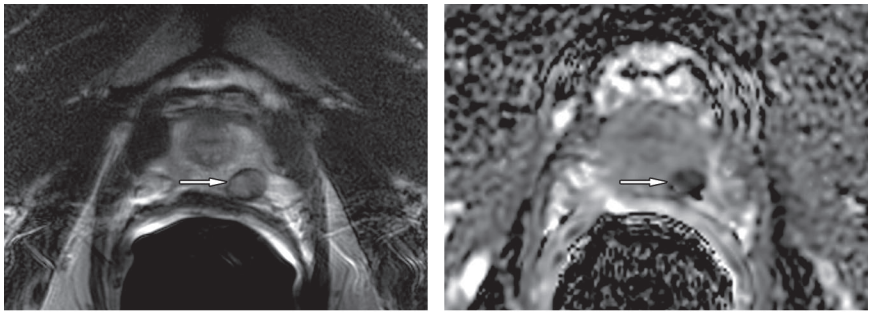

a. b.

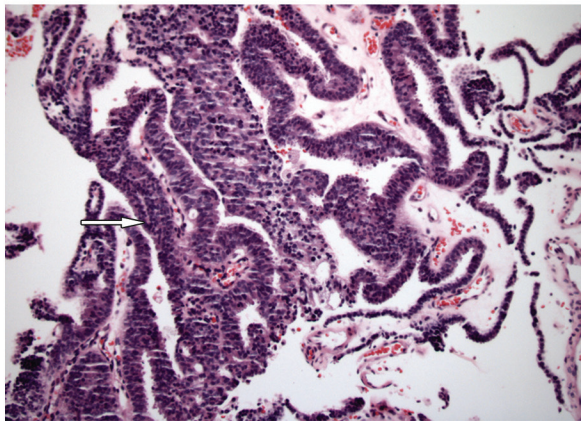

c.

reported series of 47 patients who underwent prostatectomy for mucinous adenocarcinoma, all demonstrated more-favorable long-term outcomes than average for patients with typical adenocarcinoma, controlling for stage and grade (36). Nonetheless, most mucinous adenocarcinomas manifest at a higher stage and grade than those of typical adenocarcinoma; and in the findings from the 2005 International Society of Urological Pathology (ISUP) Consensus Conference on Gleason Grading of Prostatic Carcinoma, the ISUP Grading Committee suggested that the tumor should be classified as Gleason score 8 (4 + 4), making it a high-risk tumor (37).

Primary Adenocarcinoma of the Seminal Vesicles

Primary adenocarcinoma of the seminal vesicles is a rare tumor, with only approximately 60 prior cases reported in the literature (38). Patients often present with obstructive uropathy or hematospermia but may also present with other nonspecific symptoms, including hematuria, pelvic pain, and dysuria.

At MR imaging, primary adenocarcinomas of the seminal vesicles are lobulated and heterogeneous in signal intensity. Importantly, these tumors appear confined to or centered in the seminal vesicles. This appearance serves as the main differentiator from other tumors of the prostate gland (Fig 11). Definitive diagnosis is made with the findings from biopsy, findings that must confirm the tumor to be macroscopically localized to the seminal vesicle and microscopically consistent with adenocarcinoma. These tumors show a positive staining reaction for CA-125 and cytokeratin 7 but do not show a positive staining reaction for PSA, prostatic acid phosphatase, or carcinoembryonic antigen. The negative staining reactions exclude adenocarcinomas of prostatic or colonic origin (39).

Because of the generally late manifestation, the prognosis for patients with primary adenocarcinoma of the seminal vesicles is often poor. Treatment includes radical prostatectomy, sometimes with adjuvant radiation therapy.

Neoplastic Invasion and Metastatic Disease

Metastatic involvement of the prostate gland by primary carcinomas of other organs is exceptionally rare and, when found, often arises in the context of direct extension of tumors in adjacent organs or disseminated disease involving multiple organs (40). Bladder urothelial carcinoma is the most common cancer to involve the prostate

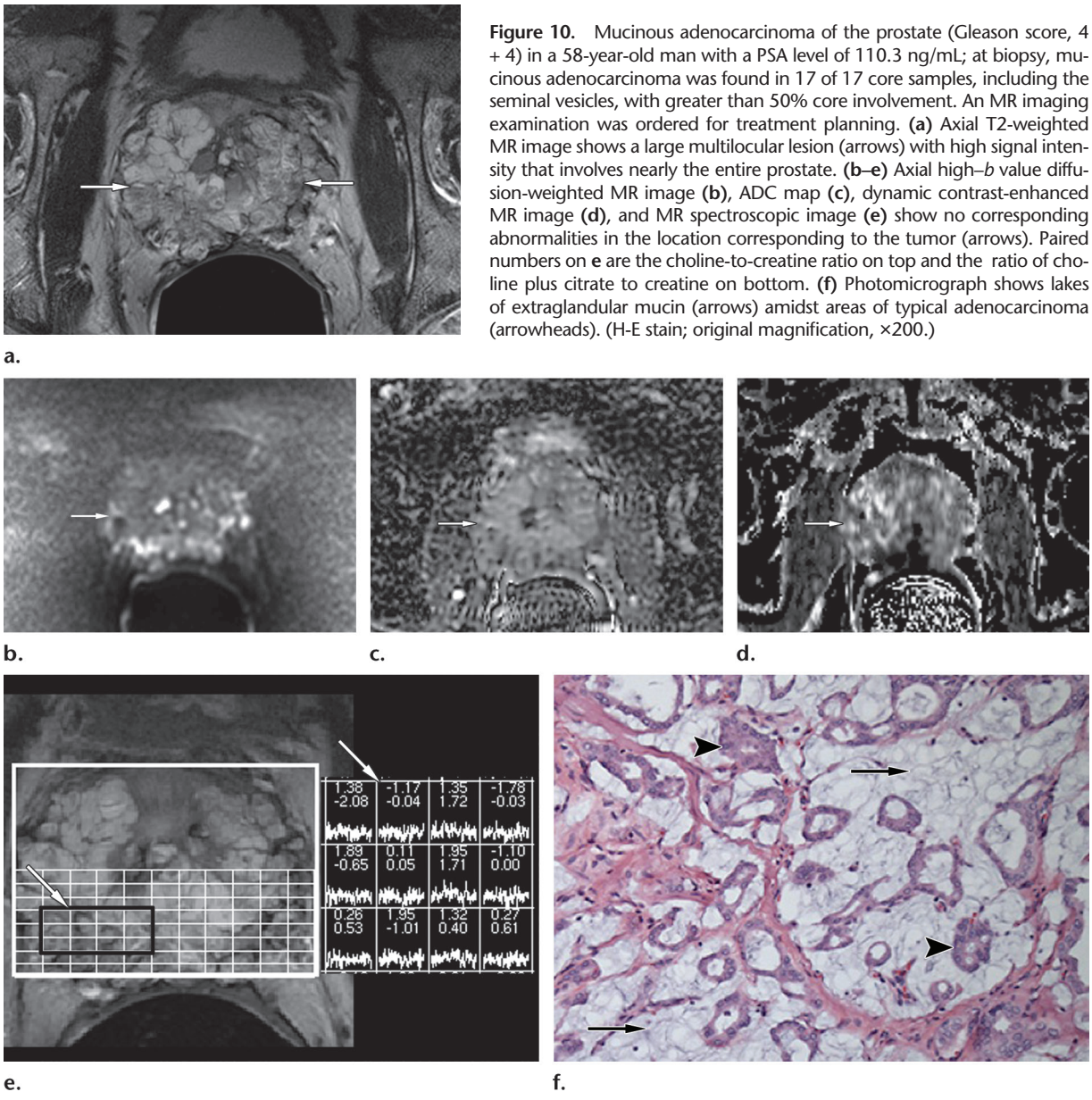

a. b. c. d. e. f.

Figure 10. Mucinous adenocarcinoma of the prostate (Gleason score, 4 + 4) in a 58-year-old man with a PSA level of 110.3 ng/mL; at biopsy, mucinous adenocarcinoma was found in 17 of 17 core samples, including the seminal vesicles, with greater than 50% core involvement. An MR imaging examination was ordered for treatment planning. **(a)** Axial T2-weighted MR image shows a large multilocular lesion (arrows) with high signal intensity that involves nearly the entire prostate. **(b–e)** Axial high–*b* value diffusion-weighted MR image **(b)**, ADC map **(c)**, dynamic contrast-enhanced MR image **(d)**, and MR spectroscopic image **(e)** show no corresponding abnormalities in the location corresponding to the tumor (arrows). Paired numbers on **e** are the choline-to-creatine ratio on top and the ratio of choline plus citrate to creatine on bottom. **(f)** Photomicrograph shows lakes of extraglandular mucin (arrows) amidst areas of typical adenocarcinoma (arrowheads). (H-E stain; original magnification, ×200.)

because of its proximity to the prostate gland. Colorectal cancer is next most frequent but is much less common (Fig 12).

Most patients with metastatic disease to the prostate present with symptoms related to their primary cancer. Only rarely are symptoms restricted to hematuria or obstructive uropathy as a result of prostatic involvement.

More than half of patients undergoing radical cystoprostatectomy for bladder urothelial carcinoma demonstrate prostatic involvement. Pathologically, urothelial carcinoma may spread to the prostate by way of urethral or ductal involvement or by direct stromal invasion, the latter being associated with a worse prognosis (41).

In some patients, distinguishing a primary colorectal cancer that invades the prostate from a primary prostate adenocarcinoma invading the rectum can be challenging. Pathologically, colorectal cancer spreads into the prostatic stroma along the prostatic ducts, mimicking prostate ductal adenocarcinoma. Colorectal adenocarcinoma shows a positive staining reaction for mucin, mimicking mucinous adenocarcinoma. PSA staining cannot be used as a reliable differentiator for whether the tumor has a prostatic origin, because primary prostatic mucinous adenocarcinoma also demonstrates a negative staining reaction for PSA (40). In patients with no known history of primary malignancy, endoscopic investigation may be helpful.

Prostatic Infections

Prostatitis, defined as inflammation or infection of the prostate gland, may be acute or chronic and may be of bacterial, viral, fungal, idiopathic, or granulomatous origin.

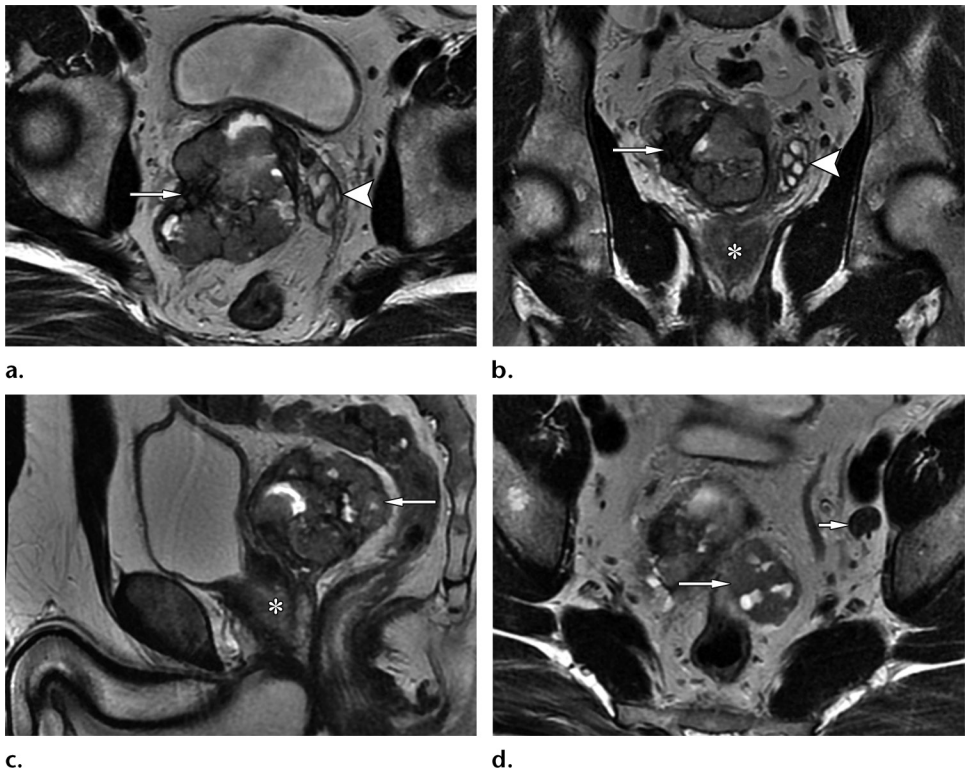

Figure 11. Primary adenocarcinoma of the seminal vesicle in a 42-year-old man who presented with right testicular pain that had been present for several weeks. The findings from physical examination and scrotal US were normal, but pelvic US disclosed a large retrovesical mass. An MR imaging examination was performed for further evaluation. Axial **(a, d)** (**a** obtained at a lower level than **d**), coronal **(b)**, and sagittal **(c)** T2-weighted MR images show a large lobulated and heterogeneous mass involving the right seminal vesicle (long arrow). The left seminal vesicle (arrowhead on **a**, **b**) and the prostate (∗ on **b**, **c**) are unremarkable. An enlarged lymph node (short arrow on **d**) of the left external iliac chain was also depicted. Transrectal US–guided biopsy and histologic examination of the prostatectomy specimen (not shown) helped establish the diagnosis of a primary adenocarcinoma of the seminal vesicle. No cancer was identified in the left seminal vesicle or the prostate.

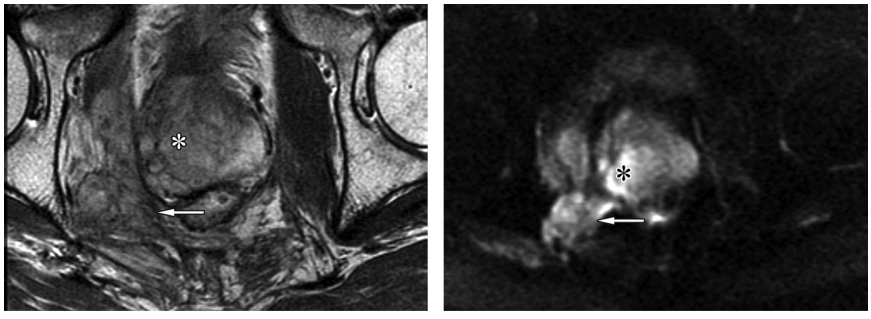

Figure 12. Rectal cancer in a 52-year-old man. An MR imaging examination was ordered for treatment planning. **(a)** Axial T2-weighted MR image shows a large multilocular lesion (∗) with intermediate signal intensity that involves nearly the entire prostate, as well as an infiltrative mass (arrow) along the right pelvic sidewall. **(b)** Axial diffusion-weighted MR image shows restricted diffusion within the tumor (∗) and the infiltrative mass (arrow). Gadolinium-based contrast material was not administered because of the patient's low glomerular filtration rate.

Pyogenic Abscess

Abscess is the most common complication of bacterial prostatitis. Patients with acute bacterial prostatitis usually present with fever and dysuria. At digital rectal examination, gentle palpation of the prostate produces pain and demonstrates fluctuation. The results of urinalysis will be positive for infection. Imaging is not usually performed in the setting of prostatitis but may be indicated to assess for complications, if the patient develops sepsis, or when pyelonephritis is suspected (42).

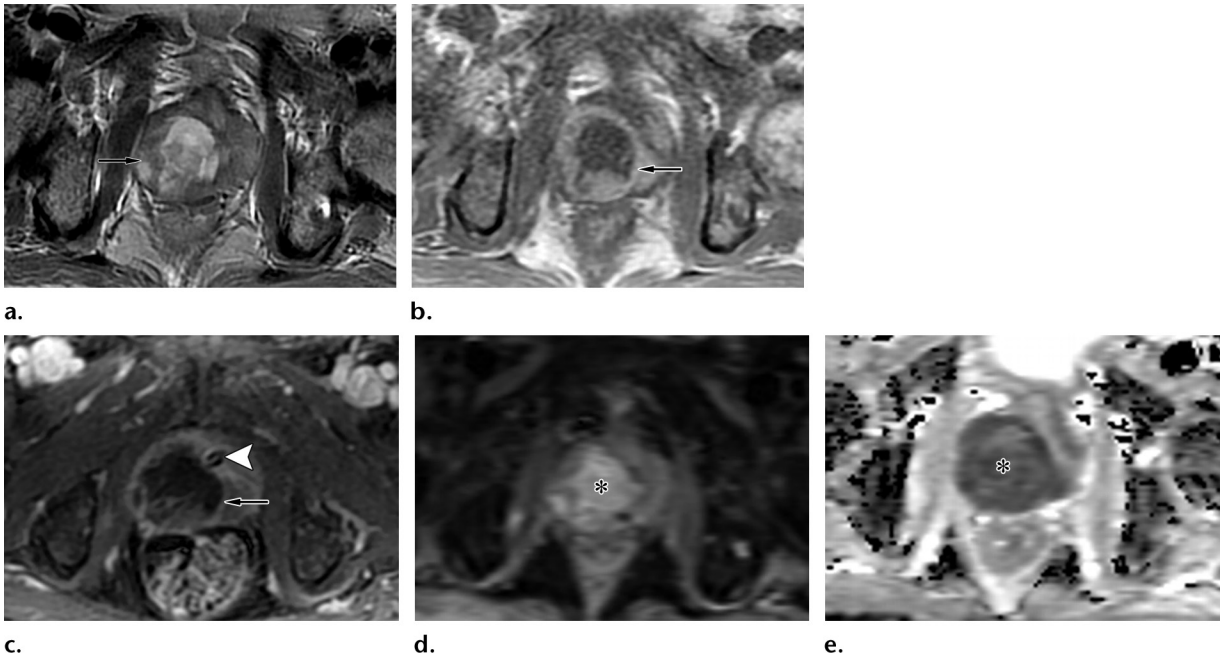

Figure 13. Abscess caused by prostatic infection in a 48-year-old man with multiple myeloma, a pathologic fracture of C2, a sacral decubitus ulcer, and persistent fevers. CT examination of the abdomen and pelvis disclosed a prostatic collection, and an MR imaging examination of the pelvis was ordered for further evaluation. **(a)** Axial T2-weighted MR image shows a heterogeneous collection (arrow) located in the central to posterior aspect of the right side of the prostate gland. **(b, c)** Axial nonenhanced **(b)** and contrast-enhanced **(c)** T1-weighted MR images show rim enhancement (arrow) of the collection before and after administration of gadolinium-based contrast material. Note the anteriorly displaced urethra and the Foley catheter (arrowhead on **c**). **(d, e)** Axial high–*b* value diffusion-weighted MR image **(d)** and ADC map **(e)** show markedly restricted diffusion (*). Imaging findings are consistent with an abscess. The patient underwent transrectal US–guided aspiration; the findings at histopathologic examination of the aspirate helped diagnose a vancomycin-resistant *Escherichia coli* infection.

Suprapubic US is generally the primary imaging modality. Identification of an enlarged hypoechoic gland with increased vascularity at Doppler US imsupports the diagnosis of uncomplicated prostatitis. When there is a prostatic abscess, a complex collection may be seen, with increased peripheral vascularity on Doppler US images. At MR imaging, prostatic abscesses are similar to abscesses elsewhere in the body; they appear as peripherally enhancing T2-hyperintense collections, with homogeneously reduced diffusion (Fig 13).

Tuberculous Prostatitis

Tuberculous prostatitis is a rare diagnosis usually made in immunocompromised patients with systemic tuberculosis or in patients who have undergone treatment with BCG infusion for bladder cancer. The genitourinary system is one of the most common sites of extrapulmonary tuberculosis, but involvement of the prostate is rare. Prostatic involvement usually occurs by way of a descending route from the kidneys or bladder or by hematogenous spread. Patients may present with symptoms related to scrotal infection, painless hematuria, or an elevated PSA level secondary to inflammation. Urinalysis often shows sterile pyuria, so a high clinical suspicion is necessary to perform staining for acid-fast bacilli.

It can be difficult to differentiate tuberculous prostatitis from adenocarcinoma at MR imaging. Both demonstrate low signal intensity on T2-weighted MR images, but tuberculous prostatitis tends to demonstrate less-pronounced restricted diffusion and absent metabolic peaks at MR spectroscopic imaging, which would be atypical for large adenocarcinomas (Fig 14) (43). Also, tuberculous prostatitis may show less-intense enhancement than adenocarcinomas (44). Ultimately, most patients undergo biopsy to exclude adenocarcinoma, but men with systemic tuberculosis or with a history of BCG infusions may be empirically treated with isoniazid and rifampin therapy. A high clinical and radiographic suspicion of tuberculous prostatitis is necessary to suggest the appropriate tests to establish the diagnosis.

Fungal Abscess

Prostatic fungal infections are commonly seen only in immunocompromised patients (45), and fungal prostatic abscesses are often seen in the setting of concomitant renal abscesses. These abscesses are indistinguishable from pyogenic abscesses on the basis of imaging alone (Fig 15), and a definitive diagnosis is often made with the results of a urine or aspirate culture. Prolonged multiagent systemic antifungal therapy is necessary

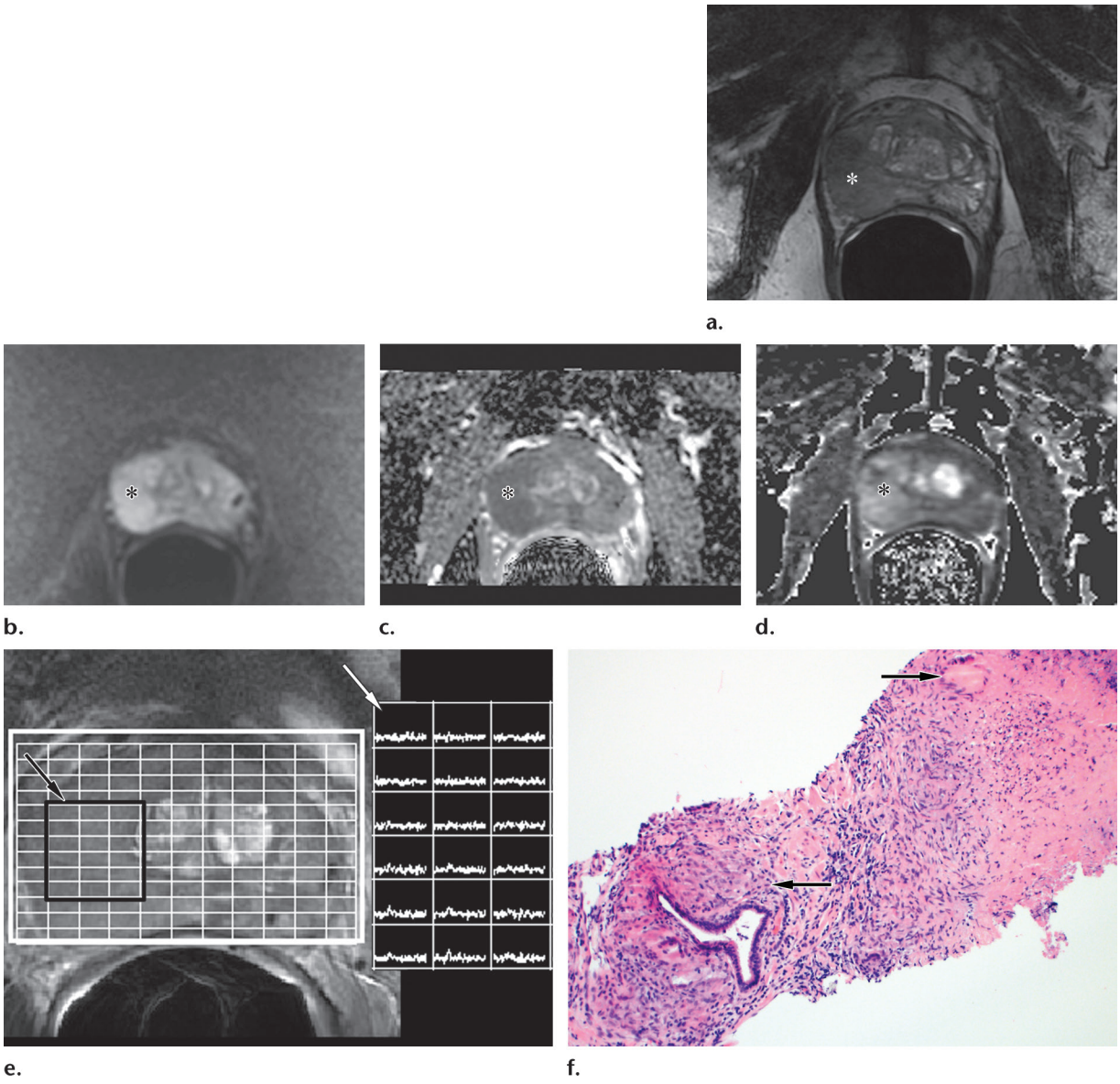

Figure 14. Tuberculous prostatitis in a 68-year-old man who had prostate cancer (Gleason score, 3 + 3) diagnosed at biopsy in one of 17 core samples, measuring 3 mm in length, involving 11% of the core sample, and who was undergoing active surveillance and had a current PSA level of 3.6 ng/mL. The patient had a history of noninvasive bladder cancer treated with transurethral resection and BCG infusion. An MR imaging examination was ordered prior to US/MR imaging fusion biopsy. **(a)** Axial T2-weighted MR image shows a 4.2-cm T2-hypointense lesion (∗) involving the right lateral peripheral zone, extending from the base to the apex. **(b, c)** Axial high–*b* value diffusion-weighted MR image **(b)** and ADC map **(c)** show that the lesion (∗) is associated with mild to moderately high signal intensity on **b** and moderately low signal intensity on **c**. **(d)** Axial dynamic contrast-enhanced parametric map shows early enhancement in the corresponding region (∗). **(e)** MR spectroscopic image, however, shows virtually absent peaks of choline, creatine, and citrate (arrows), which usually are clearly seen at different ratios in the normal prostate and in prostate cancer. Fusion biopsy was performed, and the findings were negative for prostate cancer. **(f)** Photomicrograph from histologic assessment shows granulomatous inflammation, including necrotizing granulomas (arrows). (H-E stain; original magnification, ×100.)

for treatment, particularly in immunocompromised patients (46).

Miscellaneous Benign Disorders of the Prostate

Prostatic Amyloidosis

Primary amyloidosis is a disease of uncertain causes that is characterized by extracellular deposition of amyloid. Localized amyloidosis affecting only a single organ system is rare and accounts for only about 6%–9% of reported cases (47,48). The results of recent research suggest that amyloid deposits form in the prostate gland in concretions derived from degenerate cells termed *corpora amylacea*. These concretions occur more frequently with advanced age. Proinflammatory calcium-binding proteins isolated from corpora amylacea are known to form amyloid (49). Thus, prostatic amyloidosis

Figure 15. Fungal abscess in a 59-year-old man with end-stage renal disease secondary to hypertension and diabetes mellitus who had undergone deceased-donor renal transplantation. Two years after transplantation, the patient presented with chills, weight loss, and fatigue. A 10-cm tender mass was palpated in the right lower quadrant. A contrast-enhanced CT examination was ordered. **(a, b)** Axial CT images of the pelvis (**a** obtained at a higher level than **b**) show a large heterogeneous predominantly cystic mass (* on **a**) in the inferior and posterior aspect of the transplanted kidney, as well as a complex rim-enhancing fluid collection (arrow on **b**) in the prostate. Note the invasive behavior of the infection, which is characterized by extension beyond the renal capsule (arrow on **a**) and marked secondary signs of inflammation adjacent to the kidney (arrowhead on **a**). **(c)** Coronal CT image shows the renal aspergilloma (*) and better depicts the extension of the prostatic infection (arrow). One year after imaging, the patient underwent nephrectomy of the transplanted kidney because of a persistent renal aspergilloma. **(d, e)** Low-power **(d)** and high-power **(e)** photomicrographs show a large area of liquefactive necrosis (arrow) of the renal medulla that was filled with fungi. (Grocott-Gomori methenamine-silver stain; original magnifications, ×12 in **d** and ×100 in **e**.) The prostatic infection resolved with conservative therapy.

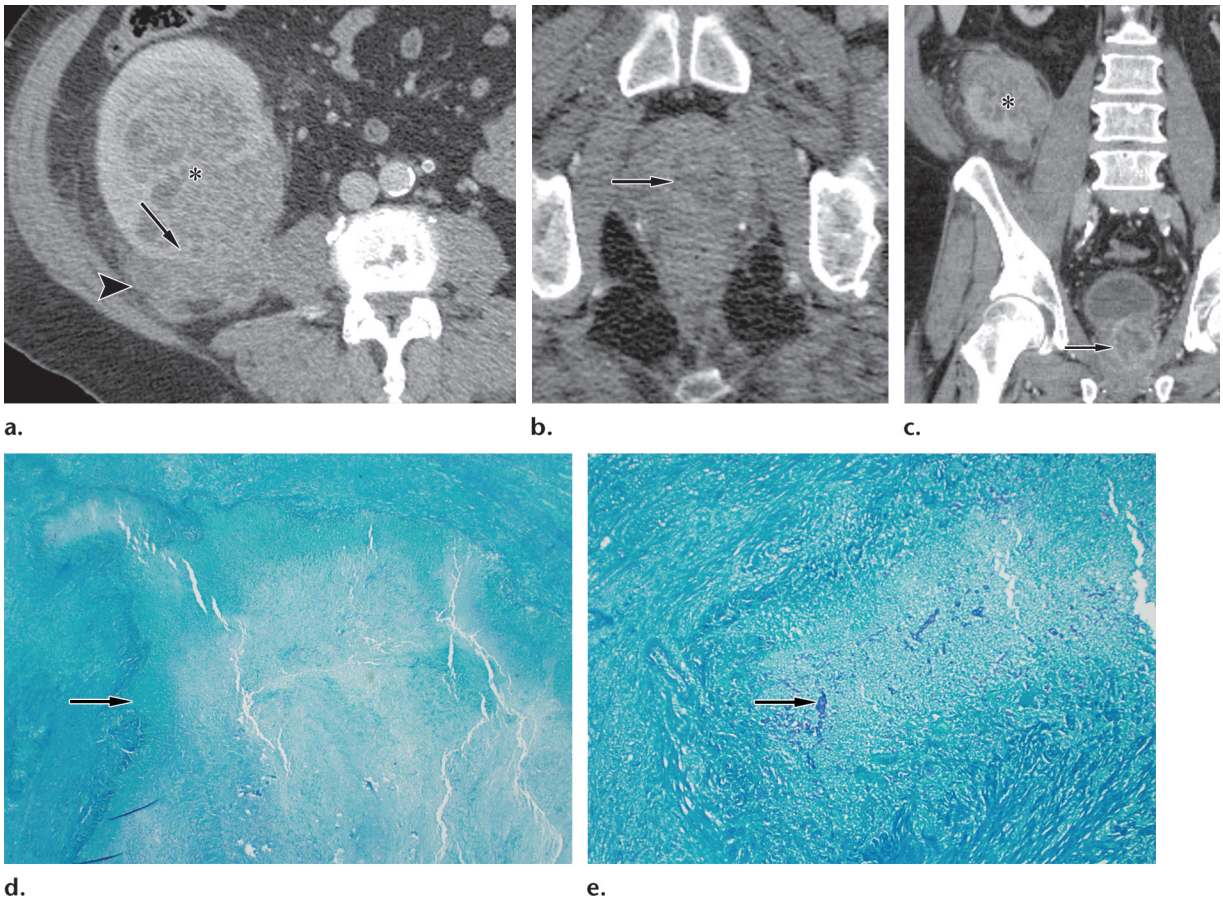

can be thought of as a secondary sign of prostate inflammation.

Similar to adenocarcinoma, prostatic amyloidosis commonly appears as a T2-hypointense mass within the prostate (50); but unlike adenocarcinoma and other aggressive neoplasms, amyloidosis does not demonstrate reduced diffusion and lacks appreciable contrast enhancement (Fig 16). Although imaging findings may be suggestive of the diagnosis, given the rarity of the disease, biopsy is still usually performed before treatment. At histologic analysis, amyloid deposits demonstrate a characteristic "apple green" coloration when examined under polarized light with Congo red staining, or they may appear violet-red with crystal violet staining (Fig 16). Often, corpora amylacea bodies can be identified with H-E staining.

When localized amyloidosis is diagnosed, a workup for systemic disease is warranted. Most commonly, patients undergo testing for plasma cell dyscrasias, such as multiple myeloma or Waldenström macroglobulinemia (51).

Prostatic Cysts

Occasionally, simple unilocular cysts can be seen in the prostate gland. Various types of cysts may occur within the prostate, all with different embryologic origins and clinical implications.

Cysts that occur in the midline of the prostate may represent a prostatic utricle cyst or müllerian duct cyst. Prostatic utricle cysts form through dilatation of the prostatic utricle, which is an embryologic remnant of the müllerian duct or urogenital sinus. Prostatic utricle cysts are always located in the midline and are often pear shaped (Fig 17). Müllerian duct cysts result from focal failure of regression and saccular dilatation of the paramesonephric duct (müllerian duct). The two

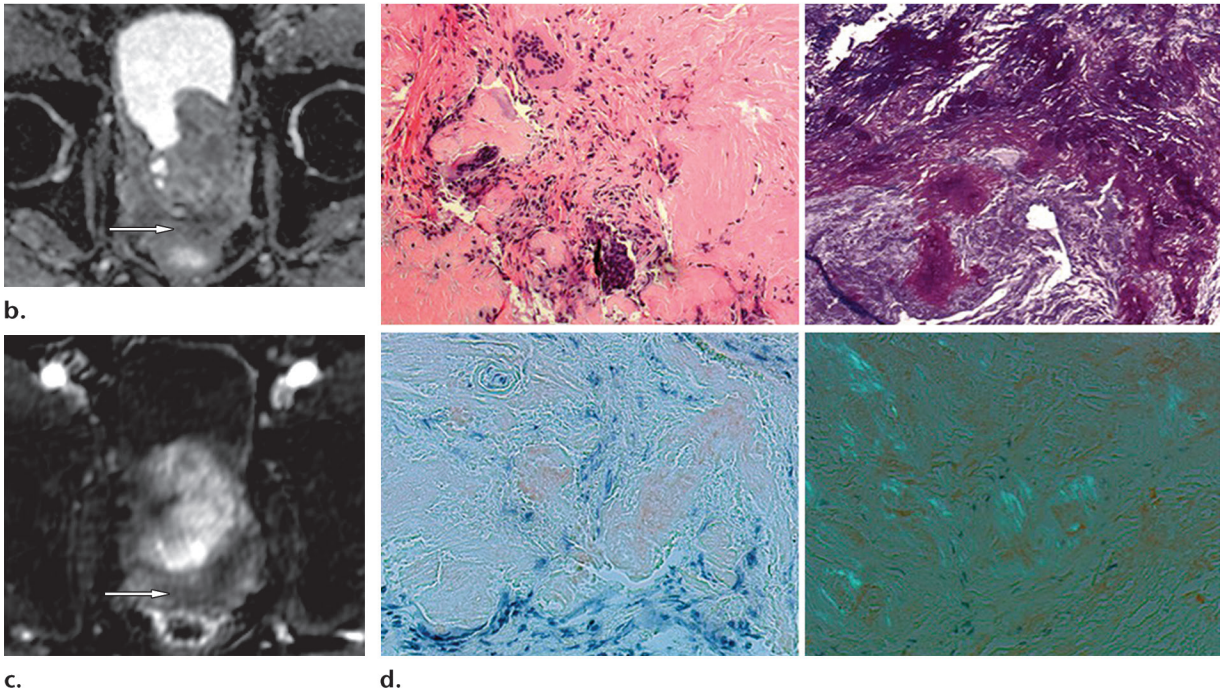

Figure 16. Amyloidosis in an 85-year-old man who was undergoing active surveillance of a low-volume prostate cancer (Gleason score, 3 + 3) in the right peripheral zone. An MR imaging examination was performed in lieu of the per-protocol transrectal US–guided biopsy. **(a)** Axial T2-weighted MR image shows a large lesion (arrow) with markedly low signal intensity in the left base peripheral zone. **(b)** ADC map shows that the lesion (arrow) had questionable restricted diffusion. **(c)** Axial contrast-enhanced MR image shows that the lesion (arrow) did not enhance after administration of gadolinium-based contrast material. A US/MR imaging fusion biopsy was performed, and the findings at histologic examination showed extensive amorphous eosinophilic deposition with giant cell reaction. **(d)** Four photomicrographs (all original magnification, ×200) obtained with various stains: *Top left,* H-E stain; *top right,* crystal violet stain; *bottom left,* Congo red stain with light microscopy; and *bottom right,* Congo red stain with polarized light microscopy. The diagnosis of amyloidosis was made on the basis of staining with Congo red and crystal violet stains. The results of hematologic and clinical evaluation excluded a diagnosis of systemic amyloidosis, and active surveillance of the patient continued without other treatments.

a.

b.

c.

d.

entities—prostatic utricle cyst and müllerian duct cyst—are virtually indistinguishable at imaging. Both are usually incidental findings but may come to clinical attention through secondary infection, hemorrhage, urinary retention, or infertility (52).

Paramedian cysts almost always represent ejaculatory duct cysts and can occur either congenitally or secondary to obstruction of the duct. Patients often present with infertility secondary to oligospermia and are found at imaging to have a small cystic lesion along the course of the ejaculatory duct. When large, these cysts may appear to arise from the midline and mimic utricle or müllerian duct cysts.

Cysts located laterally within the prostate gland may represent retention cysts or cystic degeneration of BPH. Prostatic retention cysts result from the dilatation of glandular acini secondary to obstruction of the small ducts. Such cysts usually measure between 1 and 2 cm and can be located in any zone of the prostate. They are usually seen in older patients and are difficult to distinguish from cystic degeneration of BPH, which is much more common and accounts for most cystic lesions.

In the setting of a cystic lesion in the prostate, it is important to exclude an abscess, cystic degeneration of a neoplasm, or a pseudocyst secondary to a neoplasm. Cysts will demonstrate T2 hyperintensity, no internal complexity, and no reduced diffusion. Diffusion-weighted MR images should be obtained to assess for evidence of abscess. Contrast-enhanced images should be obtained to assess for internal enhancement. If there is hemorrhage, internal complexity, or a solid component within the cyst, further workup for malignancy is warranted.

Exophytic BPH

BPH is a benign proliferation of prostatic epithelial and stromal cells of the transition zone, which form hyperplastic nodules. These nodules

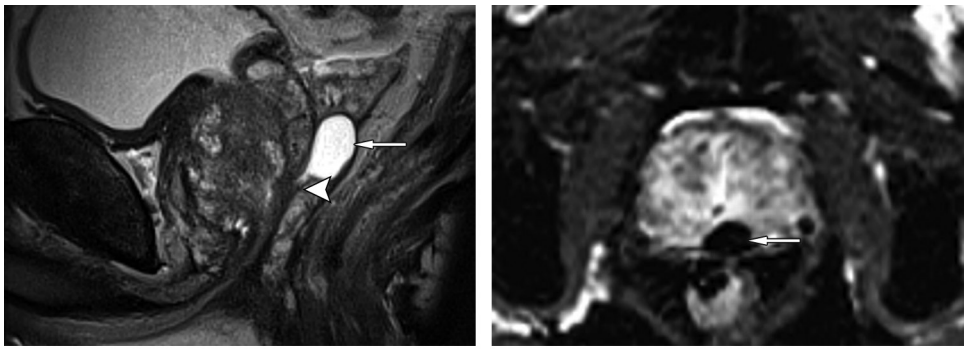

a. b.

Figure 17. Prostatic utricle cyst in a 73-year-old man with prostate cancer that was diagnosed with the histopathologic findings at biopsy, who was undergoing active surveillance. **(a)** Sagittal T2-weighted MR image shows a pear-shaped midline cystic structure (arrow) arising at the level of the verumontanum (arrowhead). **(b)** Axial contrast-enhanced MR image shows a lack of enhancement of the cyst (arrow). No reduced signal intensity was depicted at diffusion-weighted MR imaging (not shown).

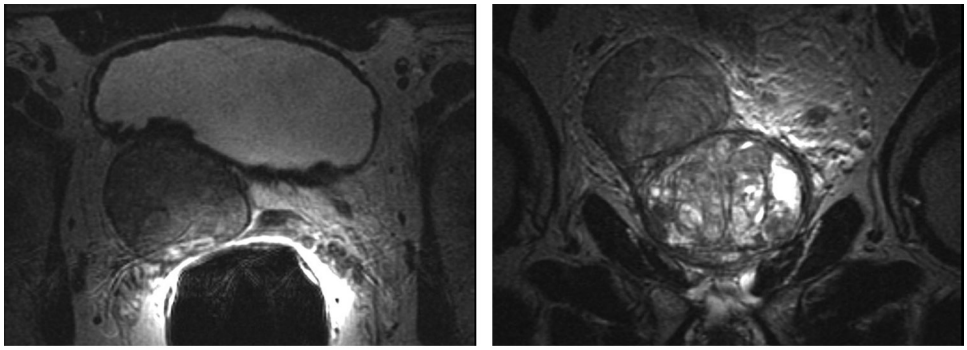

a. b.

Figure 18. BPH in a 60-year-old man with an elevated PSA level. Digital rectal examination disclosed a palpable nodule, and an MR imaging examination was ordered for further evaluation. Axial **(a)** and coronal **(b)** T2-weighted MR images show a circumscribed hypointense slightly heterogeneous encapsulated nodule, a finding consistent with BPH. The patient underwent systematic transrectal US–guided biopsy, which included sampling of the nodule, but no cancer was detected.

are most commonly seen in the transition zone but occasionally can protrude into the peripheral zone or even beyond the prostate gland and appear as an exophytic pelvic mass or a mass within the bladder (53). Exophytic BPH must be contiguous with BPH within the prostate and demonstrate similar morphologic structure and signal intensity (Fig 18). Often, biopsy is required for definitive differentiation from adenocarcinoma.

Conclusion

Although the diagnosis and staging of prostate acinar adenocarcinoma are the most common indications for performing prostate MR imaging, it is important for the radiologist to consider alternative differential diagnoses, including infection, inflammatory conditions, and less-common neoplasms. Substantial overlap can exist in the clinical history and imaging features associated with various prostate pathologic conditions, and biopsy is often required for ultimate confirmation of a diagnosis. Many diagnoses, however, including cystadenoma, mucinous adenocarcinoma, sarcomas, and abscesses, have distinct imaging features, which may alert the radiologist to the diagnosis and redirect the clinical workup and management. As prostate MR imaging becomes an increasingly common part of the prebiopsy workup of patients suspected of having prostate disease, recognition of the full range of prostate pathologic conditions at imaging will lead to more accurate and timely diagnosis and treatment.

Acknowledgments.—The authors acknowledge the help of Dominique Geoffroy, BS, UCSF Department of Pathology, San Francisco, Calif, for assistance in obtaining the pathology images and also acknowledge the help of Evis Sala, MD, PhD, Memorial Sloan Kettering Cancer Center, New York, NY; Hebert Alberto Vargas, MD, Memorial Sloan Kettering Cancer Center, New York, NY; and Andrew B. Rosenkrantz, MD, New York University Langone Medical Center, New York, NY, who shared cases from their institutions.

Disclosures of Conflicts of Interest.—**A.C.W.** *Activities related to the present article:* disclosed no relevant relationships. *Activities not related to the present article:* personal fees from 3DBiopsy. *Other activities:* disclosed no relevant relationships. **J.M.** *Activities related*

to the present article: disclosed no relevant relationships. *Activities not related to the present article:* disclosed no relevant relationships. *Other activities:* wife is an employee of Thermo Fisher Scientific. **J.S.** *Activities related to the present article:* disclosed no relevant relationships. *Activities not related to the present article:* personal and consulting fees from Genomic Health; unrestricted institutional support from Genomic Health, GenomeDx, and Myriad Genetics. *Other activities:* disclosed no relevant relationships. **S.C.B.** *Activities related to the present article:* disclosed no relevant relationships. *Activities not related to the present article:* grant from GE Healthcare. *Other activities:* disclosed no relevant relationships.

References

1. What are the key statistics about prostate cancer? American Cancer Society Web site. http://www.cancer.org/cancer/prostatecancer/detailedguide/prostate-cancer-key-statistics. Accessed February 23, 2015.
2. McNeal JE, Redwine EA, Freiha FS, Stamey TA. Zonal distribution of prostatic adenocarcinoma: correlation with histologic pattern and direction of spread. Am J Surg Pathol 1988;12(12):897–906.
3. Hosseinzadeh K, Schwarz SD. Endorectal diffusion-weighted imaging in prostate cancer to differentiate malignant and benign peripheral zone tissue. J Magn Reson Imaging 2004;20(4):654–661.
4. Noworolski SM, Vigneron DB, Chen AP, Kurhanewicz J. Dynamic contrast-enhanced MRI and MR diffusion imaging to distinguish between glandular and stromal prostatic tissues. Magn Reson Imaging 2008;26(8):1071–1080.
5. Hansford BG, Peng Y, Jiang Y, et al. Dynamic contrast-enhanced MR imaging curve-type analysis: is it helpful in the differentiation of prostate cancer from healthy peripheral zone? Radiology 2015;275(2):448–457.
6. Rusch D, Moinzadeh A, Hamawy K, Larsen C. Giant multilocular cystadenoma of the prostate. AJR Am J Roentgenol 2002;179(6):1477–1479.
7. Maluf HM, King ME, DeLuca FR, Navarro J, Talerman A, Young RH. Giant multilocular prostatic cystadenoma: a distinctive lesion of the retroperitoneum in men—a report of two cases. Am J Surg Pathol 1991;15(2):131–135.
8. Chang JM, Lee HJ, Lee SE, et al. Pictorial review: unusual tumours involving the prostate—radiological-pathological findings. Br J Radiol 2008;81(971):907–915.
9. Murer LM, Talmon GA. Stromal tumor of uncertain malignant potential of the prostate. Arch Pathol Lab Med 2014;138(11):1542–1545.
10. Herawi M, Epstein JI. Specialized stromal tumors of the prostate: a clinicopathologic study of 50 cases. Am J Surg Pathol 2006;30(6):694–704.
11. Eble JN, Sauter G, Epstein JI, Sesterhenn IA, eds. World Health Organization classification of tumours: pathology and genetics of tumours of the urinary system and male genital organs. Lyon, France: IARC, 2004. IARC Web site. http://www.iarc.fr/en/publications/pdfs-online/pat-gen/bb7/. Accessed March 8, 2015.
12. Andreou A, Whitten C, MacVicar D, Fisher C, Sohaib A. Imaging appearance of sarcomas of the prostate. Cancer Imaging 2013;13:228–237.
13. Sohn M, Kwon T, Jeong IG, et al. Histologic variability and diverse oncologic outcomes of prostate sarcomas. Korean J Urol 2014;55(12):787–801.
14. Takashi M, Sakata T, Nagai T, et al. Primary transitional cell carcinoma of prostate: case with lymph node metastasis eradicated by neoadjuvant methotrexate, vinblastine, doxorubicin, and cisplatin (M-VAC) therapy. Urology 1990;36(1):96–98.
15. Mazzucchelli R, Morichetti D, Lopez-Beltran A, et al. Neuroendocrine tumours of the urinary system and male genital organs: clinical significance. BJU Int 2009;103(11):1464–1470.
16. Parimi V, Goyal R, Poropatich K, Yang XJ. Neuroendocrine differentiation of prostate cancer: a review. Am J Clin Exp Urol 2014;2(4):273–285.
17. Lim KH, Huang MJ, Yang S, Hsieh RK, Lin J. Primary carcinoid tumor of prostate presenting with bone marrow metastases. Urology 2005;65(1):174.
18. Tash JA, Reuter V, Russo P. Metastatic carcinoid tumor of the prostate. J Urol 2002;167(6):2526–2527.
19. Wang HH, Chen YL, Kao HL, et al. Extra-adrenal paraganglioma of the prostate. Can Urol Assoc J 2013;7(5-6):E370–E372.
20. Padilla-Fernández B, Antúnez-Plaza P, Lorenzo-Gómez MF, Rodríguez-González M, Martín-Rodríguez A, Silva-Abuín JM. Paraganglioma of prostatic origin. Clin Med Insights Case Rep 2012;5:69–75.
21. Sahdev A, Sohaib A, Monson JP, Grossman AB, Chew SL, Reznek RH. CT and MR imaging of unusual locations of extra-adrenal paragangliomas (pheochromocytomas). Eur Radiol 2005;15(1):85–92.
22. Subramanian VS, Coburn M, Miles BJ. Carcinosarcoma of the prostate with multiple metastases: case report and review of the literature. Urol Oncol 2005;23(3):181–183.
23. Humphrey PA. Histological variants of prostatic carcinoma and their significance. Histopathology 2012;60(1):59–74.
24. Grignon DJ. Unusual subtypes of prostate cancer. Mod Pathol 2004;17(3):316–327.
25. Altay C, Seçil M, Demir Ö, Tuna B, Yörükoğlu K. Imaging findings of prostate carcinosarcoma: a case report. Clin Genitourin Cancer 2014;12(4):e139–e141.
26. Fukawa T, Numata K, Yamanaka M, et al. Prostatic carcinosarcoma: a case report and review of literature. Int J Urol 2003;10(2):108–113.
27. Dundore PA, Cheville JC, Nascimento AG, Farrow GM, Bostwick DG. Carcinosarcoma of the prostate: report of 21 cases. Cancer 1995;76(6):1035–1042.
28. Melicow MM, Pachter MR. Endometrial carcinoma of prostatic utricle (uterus masculinus). Cancer 1967;20(10):1715–1722.
29. Bostwick DG, Kindrachuk RW, Rouse RV. Prostatic adenocarcinoma with endometrioid features: clinical, pathologic, and ultrastructural findings. Am J Surg Pathol 1985;9(8):595–609.
30. Matsui Y, Sugino Y, Iwamura H, Oka H, Fukuzawa S, Takeuchi H. Ductal adenocarcinoma of the prostate associated with prostatic multilocular cyst. Int J Urol 2002;9(7):413–415.
31. Brinker DA, Potter SR, Epstein JI. Ductal adenocarcinoma of the prostate diagnosed on needle biopsy: correlation with clinical and radical prostatectomy findings and progression. Am J Surg Pathol 1999;23(12):1471–1479.
32. Millar EK, Sharma NK, Lessells AM. Ductal (endometrioid) adenocarcinoma of the prostate: a clinicopathological study of 16 cases. Histopathology 1996;29(1):11–19.
33. Epstein JI, Lieberman PH. Mucinous adenocarcinoma of the prostate gland. Am J Surg Pathol 1985;9(4):299–308.
34. Epstein JI, Algaba F, Allsbrook WC Jr, et al. Acinar adenocarcinoma. In: Eble JN, Sauter G, Epstein JI, Sesterhenn IA, eds. World Health Organization classification of tumours: pathology and genetics of tumours of the urinary system and male genital organs. Lyon, France: IARC, 2004. IARC Web site. http://www.iarc.fr/en/publications/pdfs-online/pat-gen/bb7/. Accessed March 8, 2015.
35. Westphalen AC, Coakley FV, Kurhanewicz J, Reed G, Wang ZJ, Simko JP. Mucinous adenocarcinoma of the prostate: MRI and MR spectroscopy features. AJR Am J Roentgenol 2009;193(3):W238–W243.
36. Guler OC, Onal C, Erbay G, Bal N. Prostate mucinous carcinoma treated with definitive radiotherapy and hormonal therapy: case report and review of the literature. Clin Genitourin Cancer 2014;12(2):e43–e46.
37. Epstein JI, Allsbrook WC Jr, Amin MB, Egevad LL; ISUP Grading Committee. The 2005 International Society of Urological Pathology (ISUP) Consensus Conference on Gleason Grading of Prostatic Carcinoma. Am J Surg Pathol 2005;29(9):1228–1242.
38. Sollini M, Silvotti M, Casali M, et al. The role of imaging in the diagnosis of recurrence of primary seminal vesicle adenocarcinoma. World J Mens Health 2014;32(1):61–65.
39. Eken A, Izol V, Aridogan IA, Erdogan S, Acıkalın A, Tansug Z. An unusual cause of hematospermia: primary adenocarcinoma of the seminal vesicle. Can Urol Assoc J 2012;6(6):E259–E262.

40. Bates AW, Baithun SI. Secondary solid neoplasms of the prostate: a clinico-pathological series of 51 cases. Virchows Arch 2002;440(4):392–396.
41. Bruins HM, Djaladat H, Ahmadi H, et al. Incidental prostate cancer in patients with bladder urothelial carcinoma: comprehensive analysis of 1,476 radical cystoprostatectomy specimens. J Urol 2013;190(5):1704–1709.
42. Schull A, Monzani Q, Bour L, et al. Imaging in lower urinary tract infections. Diagn Interv Imaging 2012;93(6):500–508.
43. Bour L, Schull A, Delongchamps NB, et al. Multiparametric MRI features of granulomatous prostatitis and tubercular prostate abscess. Diagn Interv Imaging 2013;94(1):84–90.
44. Delongchamps NB, Rouanne M, Flam T, et al. Multiparametric magnetic resonance imaging for the detection and localization of prostate cancer: combination of T2-weighted, dynamic contrast-enhanced and diffusion-weighted imaging. BJU Int 2011;107(9):1411–1418.
45. Roux C, Thyss A, Gari-Toussaint M. Prostatic and renal aspergillosis due to *Aspergillus fumigatus* in a patient receiving alemtuzumab for chronic lymphocytic leukaemia. J Mycol Med 2013;23(4):270–273.
46. Banks FC, Kelkar A, Harvey CJ, Williams G. Aspergillosis prostatitis post-renal transplantation. Nephrol Dial Transplant 2005;20(12):2865–2866.
47. Singh SK, Wadhwa P, Nada R, Mohan VC, Singh P, Jha V. Localized primary amyloidosis of the prostate, bladder and ureters. Int Urol Nephrol 2005;37(3):495–497.
48. Browning MJ, Banks RA, Tribe CR, et al. Ten years' experience of an amyloid clinic: a clinicopathological survey. Q J Med 1985;54(215):213–227.
49. Yanamandra K, Alexeyev O, Zamotin V, et al. Amyloid formation by the pro-inflammatory S100A8/A9 proteins in the ageing prostate. PLoS One 2009;4(5):e5562.
50. Ogawa Y, Nakagawa M, Ikeda S. Prostate amyloid tumor is a clue leading to the diagnosis of systemic AL amyloidosis. Amyloid 2013;20(3):193–194.
51. Picken MM, Westermark P. Amyloid detection and typing: summary of current practice and recommendations of the consensus group. Amyloid 2011;18(suppl 1):48–50.
52. Shebel HM, Farg HM, Kolokythas O, El-Diasty T. Cysts of the lower male genitourinary tract: embryologic and anatomic considerations and differential diagnosis. RadioGraphics 2013;33(4):1125–1143.
53. Blaschko SD, Eisenberg ML. Exophytic benign prostatic hyperplasia. Urology 2011;78(2):322.